

SEDIMENT DYNAMICS MODELLING IN THE RIVER SPÖL IN THE SWISS NATIONAL PARK

APPLICATION OF LINE-BY-NUMBER ANALYSIS AND DEM DIFFERENCING FOR THE GENERATION OF A 1D SEDIMENT TRANSPORT MODEL USING BASEMENT V2.3.

A MASTER PROJECT THESIS AT ETH ZÜRICH BY MATTHIAS PFÄFFLI, mpfaeffl@ethz.ch

20. DECEMBER 2013



SUPERVISION:

IfU: Prof. Dr. Peter Molnar
Hydrology and Fluvial Systems
Institute of Environmental Engineering
ETH ZÜRICH

VAW: Dr. Annunziato Siviglia

eQcharta: Dr. Michael Doering & Christian Hossli

Abstract

Hydropower production using large alpine reservoirs affects sediment dynamics and its related processes downstream of a dam. The environmental flow regime is not able to maintain natural dynamic processes throughout the year. There is a unique environmental flow management in the alpine river Spöl, located in the Swiss National Park, with regular, artificial flooding to maintain habitat diversity, and therefore also triggering sediment dynamics.

The first aim of this study was to get the grain size distributions along a 6 km long reach of the river Spöl between the dam Punt dal Gall and the lateral inflow Ova il Fuorn using the line-by-number analysis. With the grain size distributions along the reach it became possible to quantify the effects of large and numerous debris cones along the reach. It was possible to determine grain size distributions for the armoring, the sub-surface and the moving bedload layer. A total of 42 samples showed a d_m of 3.9 cm and a d_{90} of 11.1 cm for the sub-surface layer. For seven out of eleven debris cones, the d_m after the cone was smaller than upstream of the debris cones which showed that the debris cones mainly bring finer grains into the riverine system.

Second, a quantification of the erosion and deposition processes occurring within the considered reach of the river Spöl was assessed over a time period of six years. To do so two Digital Elevation Models, one from 2003 and the other from 2009, were compared with their Thalwegs and a more advanced 2D differences method. Similarly, an error propagation was carried out that showed an uncertainty threshold of ± 0.85 m. The mean elevation change between 2003 and 2009 was determined to be -1.78 m, indicating a loss of material during these six years. Also the total mass balance was calculated showing that there is a large sediment loss in the system.

The third aim of the study was the generation of a one dimensional sediment transport model using the software Basement. The calibrated model using Wu bedload transport and a multiple grain size distribution could reproduce the trends from the observations with the DEM differencing, giving even more evidence that river bed is rather eroding than aggrading. Steady-state and transient-case simulations showed that the river needs at least $5 \text{ m}^3/\text{s}$ of flow in order to show some sediment dynamic processes and that an optimal flood that triggers sediment dynamics would lie within $10 - 30 \text{ m}^3/\text{s}$. The sediment flushed out of the observed system for a mean flood with a peak of $30 - 40 \text{ m}^3/\text{s}$ ranged around 1000 m^3 . This value could be used later to calculate the aggradation in the reservoir Ova Spin.

The study showed that the line-by-number analysis can be used for roughness estimation of a river bed as well as the definition of the multiple grain size distribution of the 1D sediment dynamic model. Furthermore the DEM differencing is a useful tool to create a possibility to calibrate a model when no bedload or suspended solids measurements are available.

Content

Abstract	0
Acknowledgement	3
1 Introduction.....	4
1.1 Study objectives.....	6
2 Methods.....	7
2.1 Study area	7
2.2 Sediment dynamics in rivers	11
2.3 Data acquisition	16
2.3.1 Available Digital Elevation Models.....	16
2.4 Line-by-number analysis	17
2.4.1 General purpose.....	17
2.4.2 Transformation and evaluation.....	18
2.4.3 Sampling Sites.....	19
2.4.4 Evaluation using ArcGIS.....	20
2.5 DEM Comparison	21
2.5.1 General Purpose	21
2.5.2 DEM properties.....	21
2.5.3 Thalweg extraction	22
2.5.4 DEM subtraction.....	24
2.5.5 Error Propagation.....	24
2.5.6 Application in ArcGIS.....	25
2.6 Basement 1D Model.....	27
2.6.1 General Purpose	27
2.6.2 Mathematical model.....	27
2.6.3 Cross-section extraction.....	28
2.6.4 Calibration of the model	32
2.6.5 Validation of the model.....	35
2.6.6 Modelling tasks.....	35
3 Results.....	37
3.1 Line-by-number analysis	37
3.2 Results from DEM Comparison.....	40
3.2.1 DEM Properties.....	40
3.2.2 Thalweg.....	40

3.2.3	Erosion/Deposition pattern.....	41
3.2.4	Mass balance	45
3.3	Basement 1D Model.....	45
3.3.1	Steady-State runs.....	47
3.3.2	Transient runs.....	47
4	Discussion.....	49
4.1	Line-by-number analysis	49
4.2	DEM Comparison	50
4.2.1	DEM Properties.....	50
4.2.2	Thalweg comparison and DEM differencing	50
4.2.3	Mass balance comparison	51
4.2.4	Methodical constraints and uncertainties	51
4.3	Basement 1D Model.....	52
4.3.1	Simulations.....	52
4.3.2	Methodical constraints.....	53
5	Conclusion and Outlook	53
5.1	Line-by-number analysis	53
5.2	Digital elevation models.....	54
5.3	Basement.....	54
6	Appendix.....	56
6.1	Basement Calibration Code.....	58
6.2	Comments to the Software	61
7	List of Figures.....	63
8	List of Tables.....	64
9	Literature.....	65

Acknowledgement

I would like to thank my supervisors, Prof. Dr. Peter Molnar, Dr. Annunziato Siviglia and Dr. Michael Doering for giving me the opportunity to delve into the topics of river modelling and sediment dynamic processes in this truly extraordinary study site. A special thanks goes to Dr. Christopher Robinson who came up with the idea of this project work. In this regard I would also like to thank Lukas Vonwiller and Christian Volz for leading me to the right path using the cross-sections in Basement. I would also like to thank to Christian Häberling from the Institute for Cartography and Geoinformation for giving me the special permission to work in the Cartography-Lab.

A special thanks goes to Ruedi Haller from the Swiss National Park who made this project possible in allowing us to do field samples in the river bed of the Spöl which is only possible with a special permission. Thank you also for giving me access to the Geodatabase of the Swiss National Park. Furthermore I would like to thank Christian Hossli for his help during the field trip and his patience in carrying around and setting up experiments and metering an endless amount of stones.

I would also like to thank Sabine Trier from the Federal Office of Topography for her help in finding out when certain flight surveys for Digital Elevation Models were carried out. Furthermore I would like to thank Walter Bernegger from the Engadiner Kraftwerke who provided me the water elevation time series of the dam Ova Spin for the last ten years. Also big thanks to Michèle Oberhänsli from the Federal Office for the Environment for providing me with the runoff time series from 1974 to 2013.

1 Introduction

The share of hydropower in the Swiss domestic production is with 56% (Swiss Federal Office of Energy, 2012) higher than the world's average of around 12% (EAWAG, 2011). This high amount of produced energy has an immense influence on the river networks which are affected by dams and discharge regulations. River regulations furthermore affect habitat diversity and the aesthetics of the landscape – and it has an effect on landscape evolution by inhibiting sediment dynamic processes.

A rather special case exists in the Swiss National Park in the Canton Grisons. The park was founded in 1914 which makes it the oldest park of the European Alps. Today it covers an area of 170.3 km² and altitudes from 1400 to 3173 masl. (Swiss National Park, 2013). The Swiss National Park is considered as category 1 (strict nature preserve) by the International Union for the Conservation of Nature and therefore no exploitations are allowed.

One of the main rivers in the National Park is the Spöl that originates in Italy. For this river, hydropower utilization was already scheduled in the national park treaty from 1914, making therefore an exception to the category 1 requirements. In 1957, an official convention was negotiated which regulated the water use between Italy and Switzerland (Swiss Federal Agency, 1957). This convention paved the way for the construction of the hydroelectric infrastructure. In 1959, after a popular vote, the construction of the dams Punt Dal Gall and Ova Spin began.

From 1970 onwards, the Spöl was regulated by the minimum instream flow, the so-called environmental flow, which is released at the dam Punt dal Gall. The releases are given in Table 1 (Mürle, 2000).

Table 1: Environmental flow releases in the river Spöl since 1970

Summer release (16.05. – 30.09.)	06:00 – 18:00	2.47 m ³ /s
	18:00 – 06:00	1.00 m ³ /s
Winter release (01.10. – 15.05.)	permanent	0.55 m ³ /s

Because of this environmental flow regime, numerous effects could be observed in the river bed. Moog et al., 1993 described a large range of impacts which a regulation can have on a river. The following list shows some of the mayor effects which were observed at the Spöl (Mürle, 2000):

- Fine sediment disposal during low-flow periods
- Change of the water temperature (warmer water in summer, danger of anchor ice in winter)
- Water quality deterioration (low dilution of nutrients and contaminants)
- Influence on the aesthetics (during the tourist season, there is a higher flow through the day than through the night)
- Homogenization of the river bed, clogging
- Aggradation due to a small shear stress
- Vegetational aspects: High algal production, water plants, spreading of trees in the river bed, suppression of typical bank vegetation

Due to two operational floods to empty the reservoirs (1990 at Punt dal Gall, 1995 at Ova Spin), ecologists discovered considerable positive effects on the river regime when artificial floods were released additionally to the environmental flow (WNPK 1991, Ackermann et al. 1996). As a result of these observed positive effects, the ecologists developed a concept for a more dynamic environmental flow regime which satisfies not only the economic interests of the hydropower operator (Engadiner Kraftwerke) but also the ecological aspects and the interests of the region. The new recommended environmental flow releases are given in Table 2 (Mürle, et al., 2005).

Table 2: Recommendation for modified environmental flow release

Summer release (16.05. – 30.09.)	permanent	1.45 m ³ /s
Winter release (01.10. – 15.05.)	permanent	0.55 m ³ /s
Additional: Release of two to three artificial floods each year for 6 - 9 hours with 10 - 30 m ³ /s.		

After a three year long test phase (2000 – 2003), an independent office recommended to keep the temporary rule for the regular floods and the amended environmental flows (Swiss Federal Office of Energy, 2011).

Figure 1 shows the flow regime since 1970 with the mean discharge and the peak flow.

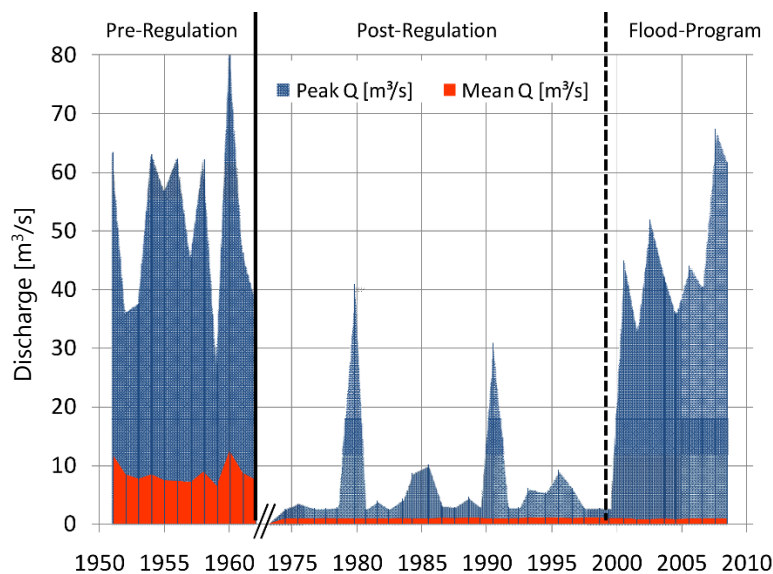


Figure 1: Hydrograph before and after dam construction and with improved environmental flow regulations (Noack, 2012)

It can be seen that until the construction of the dam there were regular floods with peaks above 50 m³/s and the mean discharge was around 10 m³/s. After the dam construction there were only two peak flows with a discharge higher than 10 m³/s and the mean discharge was reduced to something above 1 m³/s. The flow regime established after 2000 is much more similar to the natural one before 1960 with annual peaks being in the same order of magnitude.

1.1 Study objectives

In the river reach there are a lot of debris cones coming down from steep hillslopes. They bring large blocks but also a large amount of finer sediments to the river bed. The effects of those debris cones on the grain size distribution were unknown up to now. With a detailed line-by-number analysis an attempt to quantify the effects of the cones to the grain size distribution was made. With the line-by-number analysis, also the changes in the distribution from upstream to downstream were assessed and whether those changes are induced by the slope, by sorting processes or by lateral inputs through debris cones.

A second analysis carried out in this study was the comparison between two Digital Elevation Models in order to quantify whether there are erosion or deposition processes in the river bed. The study shows the limitations and uncertainties, which are associated with the use of DEMs and shows different types of comparison. Also an estimation of the total mass of eroded or deposited sediment was made, which shows whether there is a deficit or a surplus in the river reach.

A third step was the generation of a 1D model using the software Basement which was calibrated with the results from DEM differencing using roughness coefficients which were determined using the line-by-number-analysis. With this model, the stability of the bed was modeled to find out which discharge is necessary for an initiation of motion of the river bed. This could also show if there are sediment processes during the low-flow periods at all and it should give an estimate of how large a discharge has to be in order to achieve sediment dynamics.

Last but not least, different synthetic floods were simulated to have an idea of the sediment balance and to see whether there are preferred flow rates which would have high sediment dynamics but low flushing out of sediment.

2 Methods

2.1 Study area

Figure 2 shows an overview of the study area with the available hydropower infrastructure and the river Spöl.

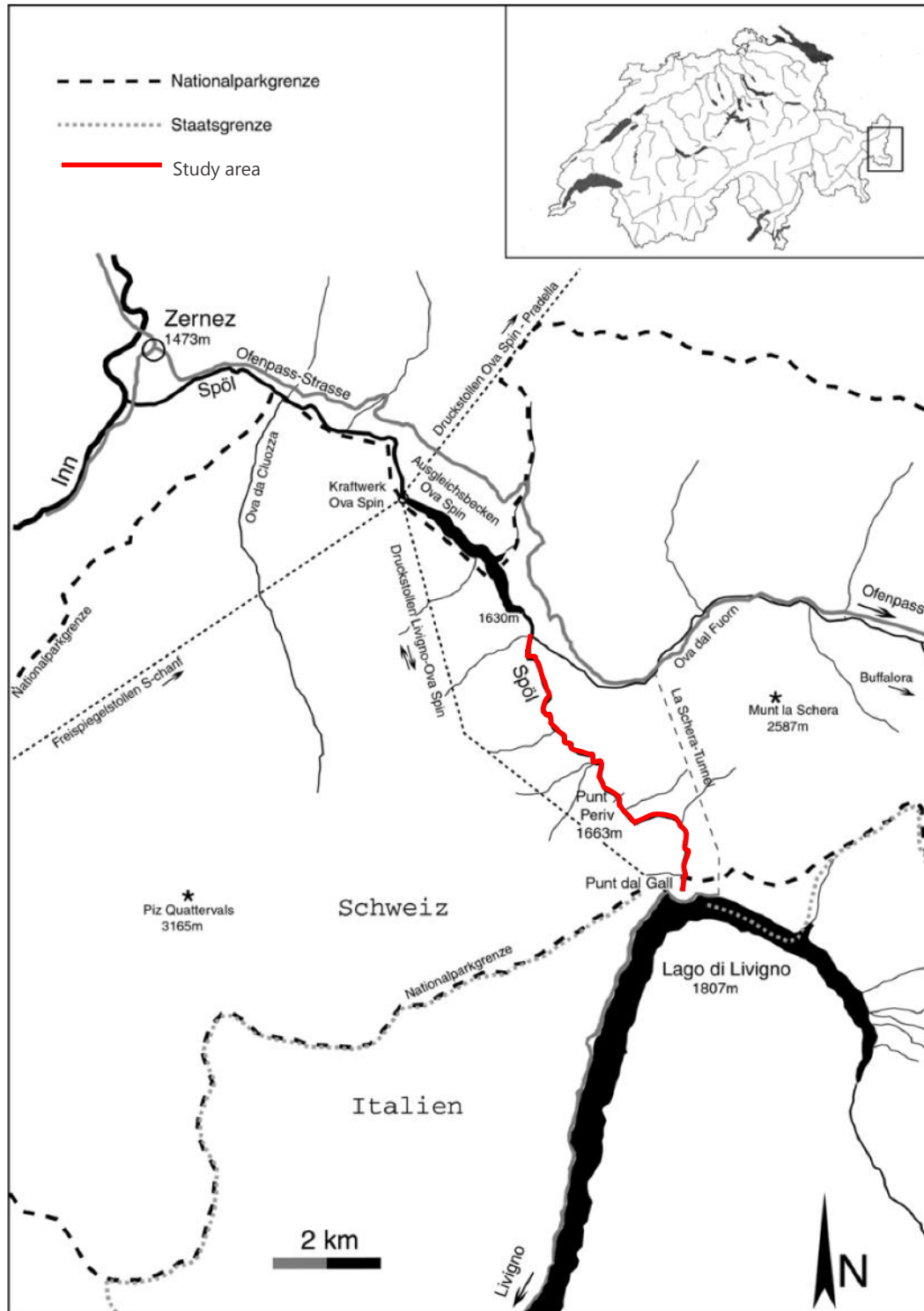


Figure 2: Overview of the study site including the hydropower infrastructure (Mürle, 2000)

The study area is located in a V-shaped valley partly having a canyon structure. The hillslopes, especially in the canyon sections, consist of pure rock. In the wider parts the hillslopes are

largely covered by trees but there are many debris cones serving as sediment sources for the river bed. The following pictures give an illustration on how the river bed looks like and how the debris cones are shaped.



Figure 3: Various debris cones (upper left: DC8, upper right: DC5, lower: DC3)

Figure 3 shows three different debris cones: The one on the upper left (DC8) is very steep and there is a lot of movement in this cone, the upper right debris cone (DC5) is at the undercut bank of the river and therefore submitted to higher flow velocities and the lower debris cone (DC3) carries a lot of fine sediments with only a few large blocks.

In the upper part of the reach there is a section, which shows a typical fluvial pattern of pools and riffles. They are shown in Figure 4.



Figure 4: Riffle-pool-sequence in the upper part of the reach

In some places, the flow is very calm and the river widens up a bit. This is shown in Figure 5.



Figure 5: Channel widening with gravel bar

In those areas, the algae growth is particularly high, covering the stones in the river bed with a light green layer. In some cases, there are even filamentous algae growing in large quantities. One of those sections is shown in Figure 6.



Figure 6: Algae growth in a return flow area

In other sections of the river, the water passes through canyons, which have solid rock on the left and the right. One of those sections is close to the end of the reach and it is shown in Figure 7.



Figure 7: Canyon like section near the End of the reach

2.2 Sediment dynamics in rivers

In a fluvial system, processes occur at a wide range of scales in space and time. The processes are not only physically based but also biologically induced. To better understand the evolution of landscapes, Schumm (1977) defined six geomorphological concepts which coexist and explain each other:

- **Uniformity**
The processes always occur under the same physical laws. The nature of the process does not change.
- **Thresholds**
The response of fluvial systems is influenced by extrinsic and intrinsic geomorphic thresholds.
- **Landscape evolution**
Landscape can be described as a balance between uplifting and erosional forces.
- **Complexity**
A fluvial system is a complex system with a behavior which is impossible to predict deterministically.
- **Self-organized critically**
The system tends to organize itself to a critical state by local instability but global stability.
- **Optimality**
The fluvial system adjusts its river network structure and channel geometry in a way that it is most efficient in transporting water and sediment.

To characterize a river in a fluvial system, one can describe its morphology, the discharge, the slope, the sediment distribution etc. The following definitions are important to characterize a river with its sediment dynamics:

a) Sediment layers

Due to flow in a gravel-carrying river, there is a separation of the material. Finer grains are more probably washed away whereas heavier grains stay on place. This sorting process leads to the generation of an armoring layer. The grains of the armoring layer often lay on top of each other like roof tiles. In this alignment, the grains have the smallest drag. Figure 8 shows an illustration of the armoring and the sub-surface layer.

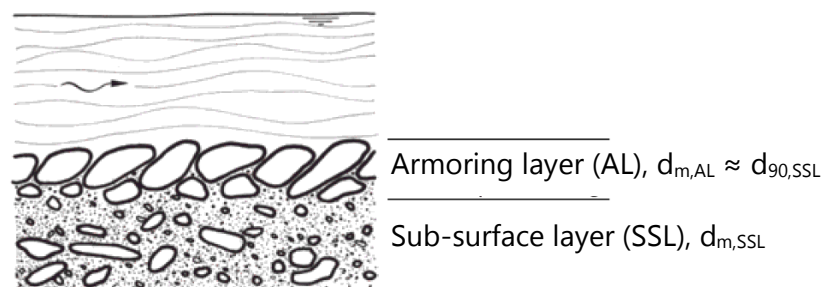


Figure 8: Armoring layer and sub-surface layer of a gravel-carrying river bed. (Patt, et al., 2011)

On top of the armoring layer, there can be moving bedload, which has a smaller d_m than the sub-surface and the armoring layer.

As shown in Figure 9, the grain size distribution varies for the sub-surface and the armoring layer. Both layers contain the same grain sizes but they differ in their frequency of occurrence.

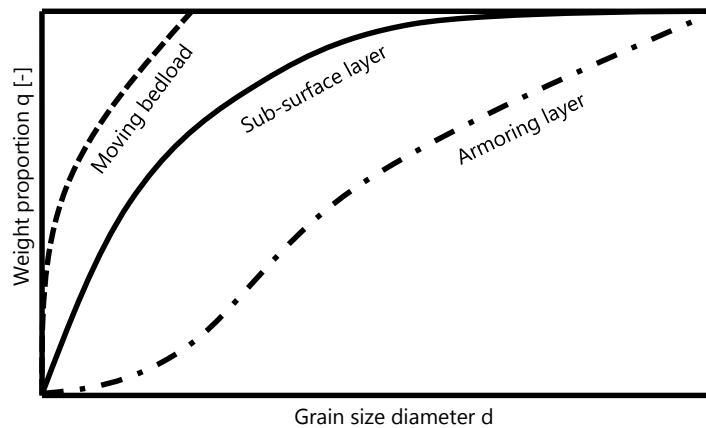


Figure 9: Grain size distribution of different river bed layers

b) Logarithmic resistance law

Experiments have shown that turbulent flow in a wide channel follows a logarithmic velocity profile. It allows the evaluation of the roughness coefficient of the stream bed based on whether smooth or rough conditions prevail in the laminar sub layer.

This approach can be adapted to narrower channels where the walls of the river influence the flow. The bed shear stress τ_0 is defined in Equation 1.

$$\tau_0 = \rho g h J \quad [1]$$

τ_0 = bed shear stress

ρ = density of fluid [kg/m^3]

g = gravity [m/s^2]

h = water depth [m]

J = slope [-]

Additionally, the shear velocity U_* is defined in Eq. 2.

$$U_* = \sqrt{\frac{\tau_0}{\rho}} \quad [2]$$

U_* = shear velocity [m/s]

The mean flow velocity in a channel by Chézy is shown in Eq. 3.

$$U_m = 2.5 \ln \frac{aR}{k_s} \sqrt{gRJ} \quad [3]$$

U_m = mean flow velocity in a channel [m/s]

a = numerical value of the profile shape [-]

R = hydraulic radius [m]

k_s = equivalent sand-grain roughness [mm]

For the above equations, a flow resistance term for the turbulent flow can be specified. The coefficient c shows the logarithmic resistance law and is defined in Equation 4.

$$c = \frac{U_m}{U_*} = 2.5 \ln \frac{aR}{k_s} \quad [4]$$

c = Chézy flow resistance coefficient [-]

The connection between the characteristic grain diameter of the armoring layer and the equivalent sand-grain roughness k_s depends on the bed of the river. The mean grain diameter of the armoring layer can be approximated by the d_{90} of the sub-surface layer.

The formula for the equivalent sand-grain roughness is shown in Eq. 5.

$$k_s = r * d_{90} \quad [5]$$

r = pre-factor depending on the river bed appearance

For single size grains on a planar or natural position, r is usually chosen to be 1 – 1.5. For multiple grain size distributions with a roof-tile like position, r is chosen to be 2. When much coarser components are available, r can be set to 3 or a different resistance law can be applied.

Another common approach to determine the average flow velocity is with a power law by Strickler (1923) (Eq. 6).

$$U_m = k_{st} R^{2/3} J^{1/2} \quad [6]$$

k_{st} = roughness coefficient [$m^{1/3}/s$]

This law can be used in the model Basement. The roughness coefficient can be derived from the equivalent sand-grain roughness k_s and the pre-factor r from Equation 5.

For a pre-factor r of 2, the relation between the two roughness coefficients are described in Eq. 7.

$$k_{st} = \frac{23.5}{\sqrt[6]{d_{90}}} \quad [7]$$

c) Initiation of motion

The motion of particles in a river bed depends on the amount of flow that is present. In a simplified, single grain bed, the sediments will start to move if the bed shear stress is larger than the critical bed shear stress. This can be calculated analytically with the equilibrium of forces. In Figure 10, the forces are shown. F_L denotes the lift force, F_D the drag force, F_R the resistance force and W_s the submerged weight (Janssen, 2010).

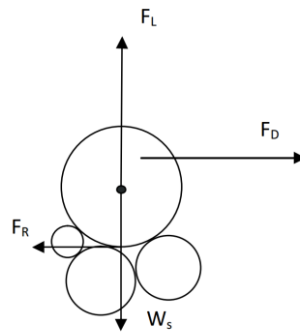


Figure 10: Balance of forces for a single particle (Janssen, 2010)

In a river there are many more than just one grain size and therefore, the equilibrium of forces is not applicable. Shields (1936) proposed an empirical relation between the dimensionless critical shear stress and the Reynolds number. The critical shear stress θ_c (also: Shields parameter) is defined in Equation 8.

$$\theta_c = \frac{\tau}{\rho g (s - 1) d}$$

s = relative density = ρ_s/ρ

d = characteristic grain diameter

[8]

The empirical relation is shown in Figure 11. The Boundary Reynolds number uses the shear velocity, which is defined in Equation 2.

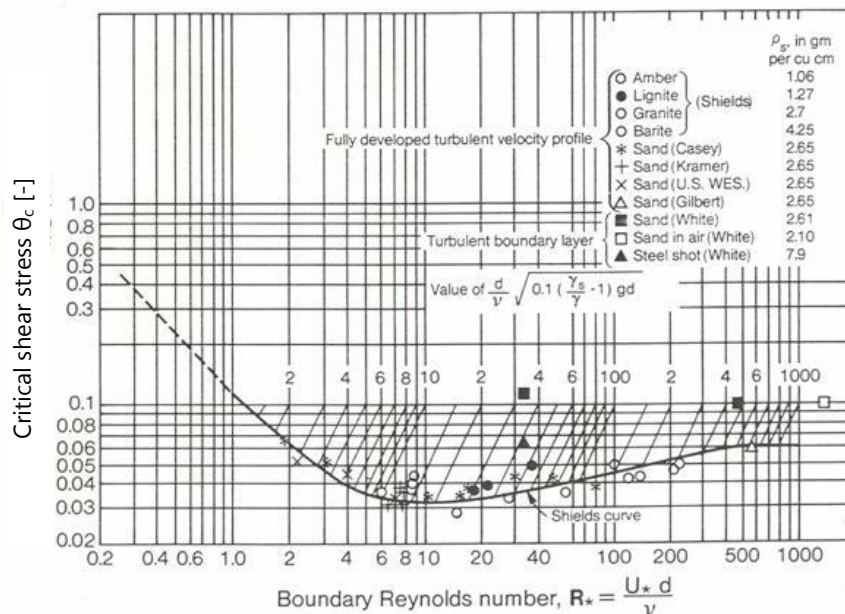


Figure 11: Shields diagram (vit13)

In gravel-carrying rivers, the Boundary Reynolds number is usually larger than 10^3 and therefore, the critical shear stress becomes constant. Shields stated the critical shear stress for the general initiation of motion to 0.06. Meyer-Peter and Müller (1948) however extrapolated with their own large-scale model a value of 0.047 which is widely used today.

d) Hiding/exposure mechanisms

In sediment mixtures, different grains size classes are in interaction between each other. Coarse particles are more exposed to flow while finer ones are commonly sheltered between the large grains (Noack, 2012). When dealing with sediment mixtures, the hiding/exposure mechanism of the river bed has to be considered. A simple hiding function for the Shields-relationship was proposed by Ferguson et al. (1989). Particles which are smaller than the mean grain diameter should have an increased Shields number whereas larger particles should have a reduced Shields number. The approach which is used in this case study is by Wu et al. (2010) who derived a formula which considers the probability for spherical grains to be exposed or hidden and defined a correction factor based on these probabilities (Noack, 2012). The following description follows closely Wu et al. (2010)

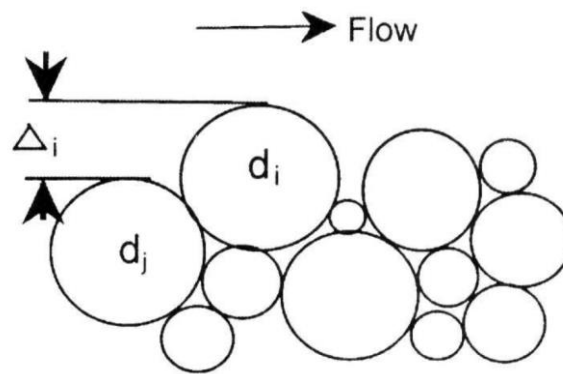


Figure 12: Definition of exposure height of bed material (Wu, et al., 2010)

In Figure 12, Δ_i defines the exposure height for a particle d_i that is the elevation difference between the particle i and its upstream particle j . If Δ_i is positive, the particle is at an exposed state, else it is in a hidden state. Δ_i is a random variable that assumedly follows a uniform probability distribution f (Equation 9).

$$f = \begin{cases} \frac{1}{d_i + d_j} & \text{for } -d_j \leq \Delta_i \leq d_i \\ 0 & \text{otherwise} \end{cases} \quad [9]$$

This probability function is used to describe the total hidden and exposed probabilities of particles by calculating the sum of all fractions (Equation 10).

$$p_{hi,j} = \sum_{j=1}^N p_{bj} \frac{d_j}{d_i + d_j} \quad p_{ei,j} = \sum_{j=1}^N p_{bj} \frac{d_i}{d_i + d_j} \quad [10]$$

p_{bj} = Percentage of particles d_j in the bed material
 $p_{hi,j}$ = Probability of particle i hidden by particle j
 $p_{ei,j}$ = Probability of particle i exposed by particle j

These probabilities are equal when a uniform grain size is considered. In a non-uniform mixture, for coarse particles, p_{ei} is larger than p_{hi} and vice-versa for small particles. This relation is used to create a correction factor, which is shown in Equation 11.

[11]

$$\Theta_{cr_g} = \frac{\tau}{\rho g (s - 1) d} = \Theta_c \left(\frac{p_{ei}}{p_{hi}} \right)^{-m}$$

Θ_{cr_g} = Critical dimensionless shields parameter for each grain class g

m = empirical number = 0.6 (Wu, et al., 2010)

2.3 Data acquisition

The following maps were acquired in order to carry out the different analyses for this project:

- **Habitat map of the Swiss National Park (HABITALP, 2008)**

"The HABITALP project deals with the diversity of alpine habitats and its goal is to monitor in a standardized way long term environmental changes in these habitats. This is performed with the help of color infrared (CIR) aerial photographs. Special focus is given to the identification and long term survey (monitoring) of NATURA 2000 sites, in particular of habitats cited in annex I of the Habitat Directive, which are detectable by aerial photographs." (Swiss National Park)

- **Orthophoto Swiss National Park**

In combination with the surveying of a LiDAR in 2009 (see Chapter 2.3.1) a high-resolution Orthophoto was acquired with a resolution of 10 cm per pixel.

For the model, an upstream and downstream boundary condition was needed.

- **Hydrograph at the station "Spöl - Punt Dal Gall (2239)"**

Right above the beginning of the river reach which is going to be simulated in BASEMENT, there is a discharge measurement station which is operated by the Federal Office for the Environment (FOEN). The time series consists of 10 min average values from January 1974 throughout October 2013.

- **Water level of the Lake "Lai dal Ova Spin"**

Below the simulated river reach, there is an equalizing reservoir from the Engadiner Kraftwerke AG. The time series consists of 10 min average elevations from January 2003 to October 2013.

2.3.1 Available Digital Elevation Models

For this project, a total of four Digital Elevation Models were acquired.

1. **DTM-AV DEM**

This elevation model was acquired by Swisstopo, the Federal Office of Topography in the year of 2003 by multiple LIDAR flights. The DEM consists of the LIDAR data for all sub 2000 masl regions. In areas over 2000 masl, the grid was supplemented by the DHM25 Level 2. The hereby used model consists of the tiles 1218 and 1238. For each tile, two flights were performed because in the first flight, there were a lot of errors which might be due to snow and ice cover. The second flight was carried out to eliminate the surface discrepancies and errors. The following Table 3 shows an overview of the flights.

Table 3: Overview of the flights for the DTM-AV DEM

Tile 1218	1 st flight: June 2003
	2 nd flight: September 2003
Tile 1238	1 st flight: May 2003
	2 nd flight: September 2003

2. swissALTI3D

The swissALTI3D is a regularly updated digital elevation model from the Federal Office of Topography in an interval of six years. In the project area, the swissALTI3D was created in the year 2009. The basis for the model are the LiDAR data from the DTM-AV of 2003 which were recompiled on the basis of up-to-date Orthophotos.

3. LiDAR 2009 SNP

The Swiss National Park executed in cooperation with the Engadiner Kraftwerke AG a very accurate LIDAR flight in the early summer of 2009. Combined with the LIDAR acquisition, also a high-resolution Orthophoto was recorded.

4. DGM2m

The DGM2m was created from many different existing model extents which were acquired by Switzerland, Italy and Austria. The goal was to have a homogeneous elevation model of the full extent of the Swiss National Park (Dusza, 2010). The component of the DEM which is used in this study consists of a modification of the DTM-AV from 2003 and especially in the border region to Italy (Punt dal Gall dam) it is overlapped with the Lomb_dtm_20, the Italian elevation model for the Lombardy.

The following Table 4 shows the general properties of those four Elevation Models:

Table 4: Overview and properties of the available DEMs in the project area

Name	Date of Inventory	Grid size	Coordinate System	Std. Dev.
DTM-AV	Spring and partly summer 2003	2 x 2 m	CHLV03/LN02	0.5 m
swissALTI3D	During 2009	2 x 2 m	CHLV03/LN02	0.5 m
LiDAR SNP	20.06.2009	1 x 1 m	CHLV03/LN02	0.06 m
DGM2m	2003 – 2010	2 x 2 m	CHLV03/LN02	unknown

During the analysis it became clear that only the models DTM-AV and the LiDAR SNP will be used for a DEM comparison. The swissALTI3D is only a digital revision from the DTM-AV data of 2003 – and it is also dated from 2009. The DGM2m is largely based on the DTM-AV data as well and additionally it is modified in various (unknown) ways giving an unknown uncertainty of the values.

2.4 Line-by-number analysis

2.4.1 General purpose

The line-by-number analysis is a simple tool to acquire samples of grain size distributions. The application is easy, quick and the results also include information about the randomness of the grains.

For the line-by-number analysis, a cord or a tape measure is stretched on a gravel bar – if possible aligned in flow direction. The b-axis of all grains, which lie below the cord are measured and allocated to different grain fractions (Form, see Figure 42). The fractions should have a geometric regression with the quotient of $\sqrt{2}$. Grains with a b-axis of less than 1 cm are neglected in the field because it is difficult to include them all and measure them correctly. This fraction is added later using a Fuller-distribution (Fehr, 1987). If time and space allows it, multiple samples should be taken on each gravel bar to compare the deviations and calculate the average.

2.4.2 Transformation and evaluation

To evaluate the line-by-number analysis samples, the frequency distribution has to be transformed to a weight distribution and additionally transformed to represent the sub-surface layer below the armoring layer. This description largely follows Bezzola, 2013.

First, the distribution of the grain classes has to be transformed from distribution samples to volume samples. This transformation is done with Eq. 12.

$$\Delta p_i = \frac{\Delta q_i d_{mi}^{0.8}}{\sum_1^N \Delta q_i d_{mi}^{0.8}} \quad [12]$$

Δp_i = relative weight of fraction i
 Δq_i = relative number of fraction i
 d_{mi} = characteristic/mean grain diameter of fraction i
 N = total number of fractions

The now obtained volume distribution has to be corrected to also include the previously neglected grains which are smaller than 1 cm. It is assumed that 25% of the grains in the study area have a b-axis of less than 1 cm which leads to the correction term in Equation 13.

$$p_{iC} = 0.25 + 0.75 \sum_1^i \Delta p_i \quad [13]$$

p_{iC} = Corrected cumulative frequency of fraction i

The 25% fines are calculated using a Fuller distribution. The goal is to find a Fuller distribution which has the same tangential slope as the converted and corrected grain size distribution. The choice of the tangential point is to a point subjective but the following procedure shows the calculation scheme which was used in this project.

First, the Fuller distribution at the point $i+1$ is calculated with Equation 14.

$$p_{FU(i+1)} = \sqrt{\frac{d_{i+1}}{d_{maxFU}}} \text{ with } d_{maxFU} = \frac{d_i}{p_{iC}^2} \quad [14]$$

$p_{FU(i)}$ = Fuller distribution of fraction i
 d_{maxFU} = Maximum grain diameter

The received distribution is now compared with the previously determined p_{iC} and the fraction i where $p_{FU(i)}$ and p_{iC} are the closest is defined as u.

Fraction u now defines the maximum grain diameter which will be used in the grain size distribution. Additionally, it defines the shape of the Fuller distribution as it is a part of Eq. 11. The fuller distribution is calculated according to Eq. 15.

$$p_{iFU} = \sqrt{\frac{d_i}{d_{maxFU}}} \text{ with } d_{maxFU} = \frac{d_u}{p_{uC}^2} \quad [15]$$

p_{iFU} = Fuller distribution of fraction i
 d_{maxFU} = Maximum grain diameter

The final grain size distribution is obtained with using the Fuller distribution up to the defined fraction u and from there on use the corrected and converted grain size distribution.

Now that the final grain size distribution is calculated, one can define various characteristic grain diameters which will be used for further analysis.

To find the mean diameter d_m , the mean diameter of each fraction i is multiplied with the corresponding weight component.

$$d_m = \int_0^1 d_{mi} dp = \sum_1^i d_{mi} \Delta p_i \quad [16]$$

d_{mi} = mean grain diameter of fraction i
 Δp_i = weight component of fraction i

Other characteristic grain sizes like the d_{90} can be interpolated from the grain size distribution.

The various roughness coefficients like the equivalent sand-grain roughness k_s , the roughness coefficient k_{st} and the manning coefficient can be calculated using the methods described in Chapter 2.2 c).

The grain size distribution of a river is not only influenced by the lateral inputs but also by the slope of the river. A steeper slope results in a higher flow velocity and a higher shear stress (Equations 1 and 6). To see whether the slope has a direct influence to the grain size distribution, it was assessed for every sample point along the river using the Thalweg of the LiDAR DEM from 2009. The slope is taken as an average from the 100 m above and the 100 m below the sample.

2.4.3 Sampling Sites

During the field survey, a total number of 42 line-by-number analysis samples were acquired. The transformation from the number of grains per grain class to a grain size distribution which uses a Fuller curve as an approximation is shown in the Appendix (Table 12).

Not only the mean grain diameter d_m but also the characteristic d_{90} was assessed. Figure 13 shows the perimeter of the river with the grain size sample points and the debris cones.

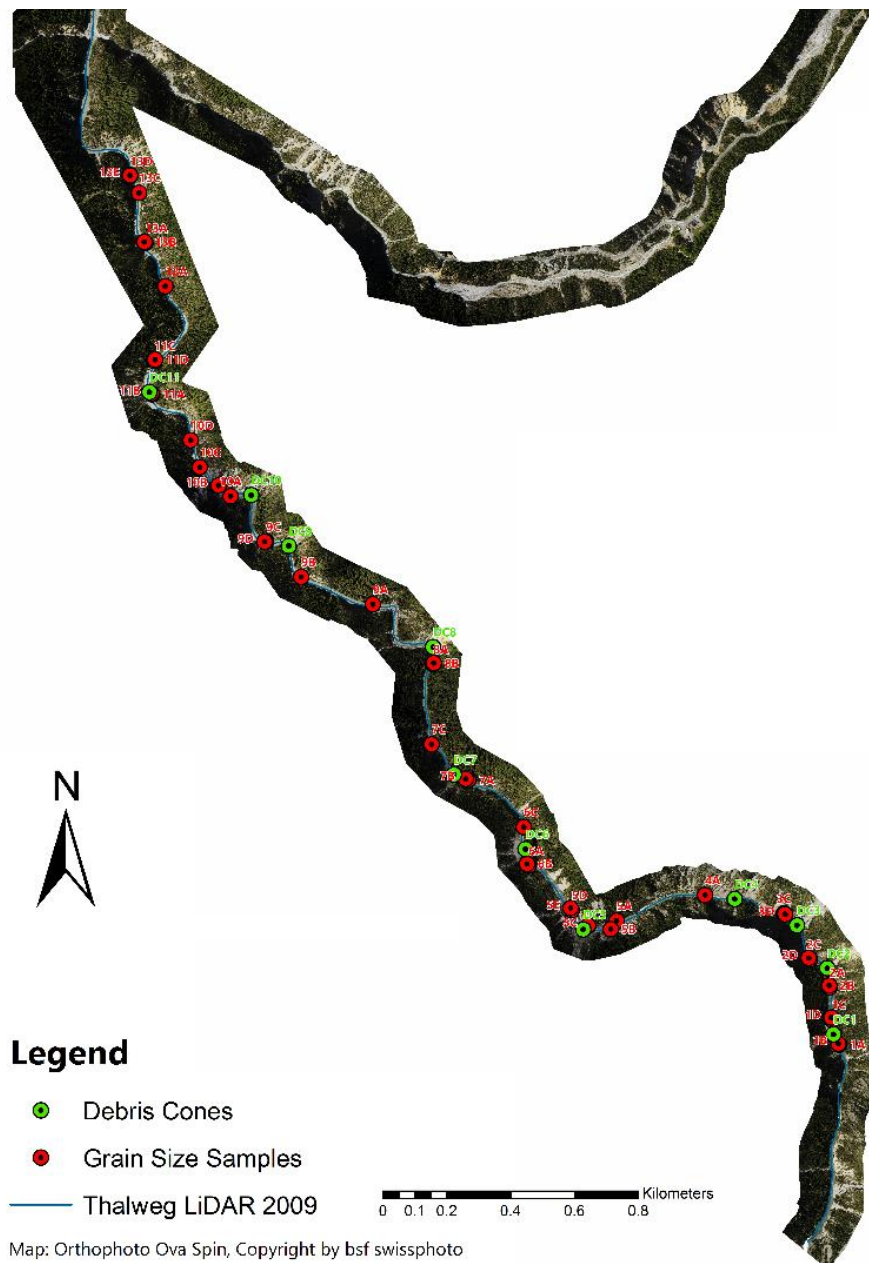


Figure 13: Overview of the river reach with the acquired grain size samples and the observed debris cones (Map: Orthophoto Ova Spin, © bsf swissphoto)

On the lower right corner of Figure 13 is the dam Punt dal Gall. The reservoir Lai dal Ova Spin is situated on the upper right corner. It can be seen that the line-by-number analysis samples were taken quite regularly over the whole reach but there are some places where no sample was taken because the river was not accessible or there were no gravel bars.

2.4.4 Evaluation using ArcGIS

During the inventory on the field, the points where the samples were taken were marked on the Orthophoto from 2009. Those points were imported into ArcGIS and they were snapped to the River Centerline from the LiDAR 2009 (see 2.3.1). To get a spatial distribution, the Centerline had to be converted from a line to a route. To do this, the polyline needs to have an additional attribute as an identifier, which can be done with the *Add Field* command in the attribute table. Then, the route can be created with *Linear Referencing Tools-Create Routes*. With *Linear Referencing Tools-Locate Features Along Routes*, the debris cone points and the grain size

sample points can be snapped in a rectangular form to the route and new points are created on the route. This tool also creates an output table with the distances between each point on the route.

Not only are the point values interesting but also the spatial pattern of the roughness distribution. Therefore the points were interpolated across the river bed using the kriging approach. The tool *Spatial Analyst Tools-Interpolation-Kriging* was used with universal kriging and a linear with linear drift semivariogram model. The resulting Kriging-raster was clipped with the tool *Data Management Tool-Raster-Raster Processing-Clip* to the extent of the river bed.

The results are however in a range of accuracy which cannot be performed with taking samples in nature. This spatial extrapolation only shows the general shift of the roughness along the reach.

2.5 DEM Comparison

2.5.1 General Purpose

The goal of the DEM Comparison is to get an estimate of erosion or deposition along the river reach between the dam Punt dal Gall and the lateral inflow from Ova il Fuorn. This is also the river reach modeled later using Basement 1D. The length of the reach is around 6 km.

With the information about how much erosion or deposition there is in the reach, one can calibrate the 1D model to get approximately the same amount of erosion or deposition for this timespan.

2.5.2 DEM properties

In order to be able to compare different elevation models, it has to be ensured that they were surveyed under the same conditions. Especially when looking at a river section of an elevation model, the conditions may vary due to the fact that the laser pulses are not able to fully penetrate the water and that the reflection of the water surface might influence the results.

The evaluation of the two elevation models DTM-AV and LiDAR 2009 is rather difficult. There is no Orthophoto which shows the conditions of the ground during the DTM-AV flights. The evaluation can only be done with the available upstream hydrographs but they too are difficult to compare because for the DTM-AV there were two flights in different months and no exact date of the flights are available. For the LiDAR 2009, there is a matching Orthophoto available and an exact flight date.

Figure 14 and Figure 15 show the hydrographs of the period where the two DEMs were surveyed.

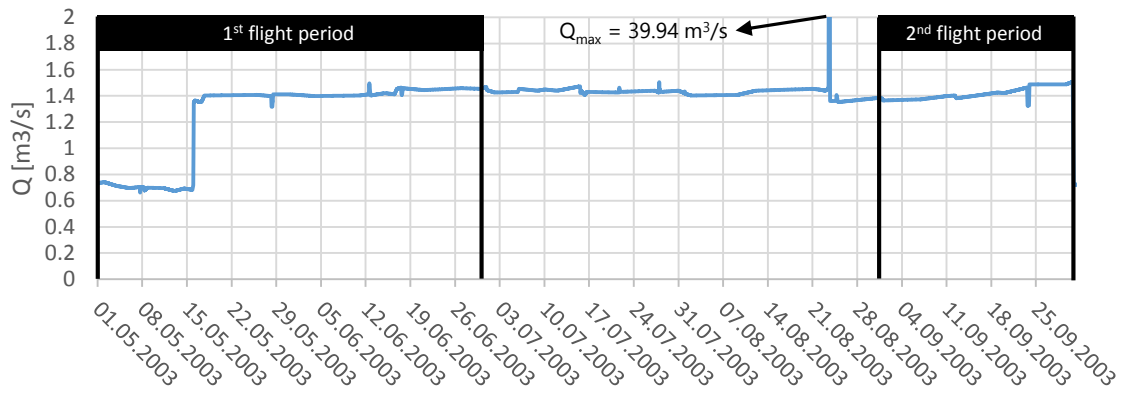


Figure 14: Hydrograph of Station "Punt dal Gall" from May - September 2003

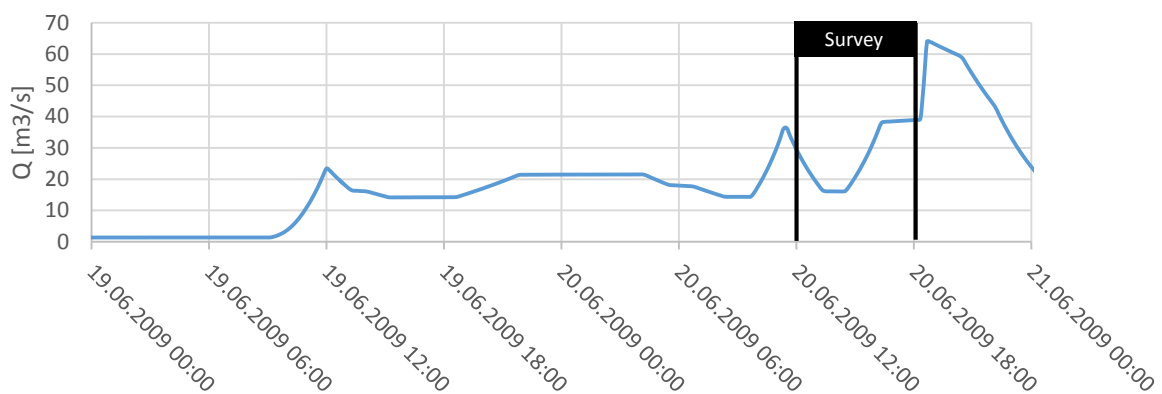


Figure 15: Hydrograph of Station "Punt dal Gall" from June 19 -20, 2009

The acquisition of the DTM-AV was consistently in a low-flow period with a discharge of 1 - 2 m³/s. However, the flight for the LiDAR 2009 survey was carried out during an artificial flood period. The flight was carried out in the afternoon of June 20th, which means that the flow at that time was around 20 m³/s.

2.5.3 Thalweg extraction

In river engineering, the Thalweg is an important feature to look at when the temporal evolution of a river section should be assessed. The Thalweg describes the lowest point of a river bed in a longitudinal profile.

When comparing different Thalwegs from different times, assumptions about erosion and deposition can be made along the river reach. Usually, the Thalwegs are created from cross-sections, which are regularly measured at the same place by total stations. In this case, there are only locally some cross-sections available (Noack, 2012 & Mürle 2000) which means that the Thalweg has to be extracted from the Digital Elevation Models.

One way to get a Thalweg from a Digital Elevation Model is to carry out a watershed analysis. This analysis derives the river network from the topography using various tools described below:

As a first step, the available DEMs have to be reviewed if they can be used to create flowpaths. A flowpath needs to continue throughout the watershed and it has to reach the lowest point of the valley from the DEM. Therefore, a DEM should not have sinks or holes. If the DEM has

holes with missing data, they have to be filled using the *Spatial Analyst Tools-Map Algebra-Raster calculator* with the command "Con(IsNull("DEM"), FocalStatistics("DEM", NbrRectangle(2, 2, "CELL"), "MEAN"), "DEM")". This command fills the missing data with a mean value which is taken from a rectangle with width and height of two cells. The existing sinks have to be filled using the *Spatial Analyst-Hydrology-FILL* tool.

In a next step, the flow direction of the cells are determined using the *Spatial Analyst-Hydrology-FLOW DIRECTION* tool. The process is visually shown in Figure 16. The output of this tool is an integer raster with defined values 1-2-4-8-16-32-64-128. Each number defines the flow direction of the raster.

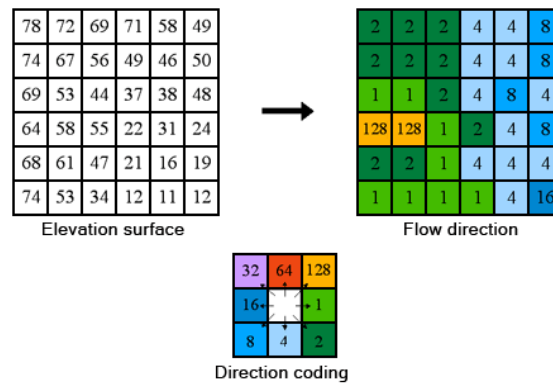


Figure 16: Flow Direction calculation steps (ESRI)

The tool *Spatial Analyst-Hydrology-FLOW ACCUMULATION* generates a raster which shows the number of cells flowing into the given cell excluding the cell itself. This raster is the basis of the river network.

Using the *Spatial Analyst-Map Algebra-Raster Calculator* a rasterized river network can be created. A threshold a_t has to be defined which expresses how many cells need to drain into a given cell in order to call this cell a river cell. This threshold may vary for the different elevation models due to their different resolution and spatial extents. The command in the raster calculator is ""FlowAcc_DEM" $\geq a_t$ ". This results in a raster with 0 for No-River and 1 for River Cells. This raster file can be transformed with the *Spatial Analyst Tools-Hydrology-STREAM TO FEATURE* tool. To make this tool work, the previously obtained raster with 0/1 cells has to be reclassified to NoData/1 cells using *Spatial Analyst Tools-Reclass-RECLASSIFY*.

The result of this analysis is a river network polyline which should represent the natural flow regime. In most cases, a river is flowing in the steepest part of a valley and the Thalweg represents the deepest point of the river bed. Therefore the extracted river network from the DEM can be used as a Thalweg of the river.

Up to this point, the Thalweg is a simple 2D line. To transform this line into a longitudinal profile, the tool *3D Analyst Tools-Functional Surface-Interpolate Shape* can be used. The basis for the elevation of each Thalweg is their filled DEM's. In this case, not the raw DEM is used because the flow paths are extracted from the filled DEM's. If the raw elevation models would have been used, the flow paths might have been different.

Each Thalweg has a different distance from top to bottom to the reach due to fluctuations in the river bed. The distance of the reach was normalized for each Thalweg using a pre-defined,

simplified Centerline. Figure 17 shows the fluctuating Thalwegs of each elevation model and the stream centerline.

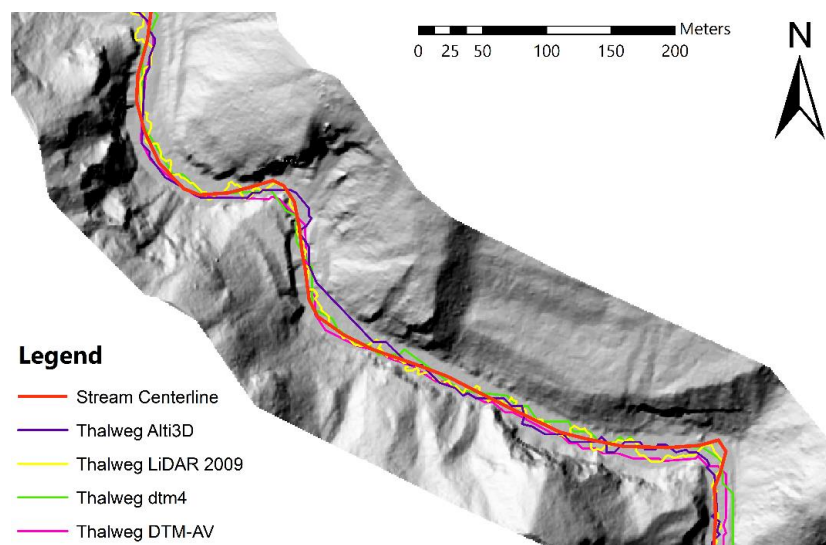


Figure 17: Extract of the river Spöl, showing fluctuating Thalwegs and the defined Stream Centerline (Map: LiDAR Ova Spin © bsf swissphoto)

2.5.4 DEM subtraction

To identify erosion and deposition patterns, one should not only look at the deepest point of a valley (Thalweg) but also at the changes of the whole river bed area. For this purpose, DEM's of difference can be created by subtraction of DEM pairs. In such an analysis, the error propagation must be included in the interpretation of the results.

The elevation models all have different spatial extents. The LiDAR covers the river with an extent of around 200 m whereas the DTM-AV which was used for the comparison covers the area in a rectangular form. To simplify the spatial extent, the subtraction of the DEMs is reduced to a manually created river bed perimeter.

The river bed perimeter was created on a visual basis using the high resolution Orthophoto from 2009. A more advanced way would be to let the model run a bankful discharge and define the river bed with the contour line which the water leaves. This would require a 2D model and is therefore not possible in this case. This "River Polygon" is also used for the main channel area definition in HEC-GeoRAS.

The DEM's used are the DTM-AV from 2003 and the LiDAR from 2009. The missing data points were filled with the same command as explained in Chapter 2.5.3 but the sinks were not filled because this would have an influence to the results.

2.5.5 Error Propagation

It is important to be able to identify erosion and deposition patterns which are not assigned to random errors from the DEM generation. Two quantities (x and y) are measured which are only subject to random errors, the assumption can be made that the quantities will be normally distributed and they can be defined by their means and standard deviations (Lane, et al., 2003).

When computing the difference of the two quantities $q = x - y$, the standard deviation of d is defined in Eq. 17.

$$\sigma_q = \sqrt{\sigma_x^2 + \sigma_y^2} \tag{17}$$

σ_q = Standard deviation of difference d
 σ_x = Standard deviation of DEM x
 σ_y = Standard deviation of DEM y

This Equation 17 can be applied as long as the different raster have the same resolution. When coarsening a grid, the standard deviation of the grid also changes (see Eq. 18).

$$\sigma_{new} = n * \sigma_{old} \tag{18}$$

σ_{new} = Standard deviation of coarsened grid
 σ_{old} = Standard deviation of original grid
 n = Number of old grid cells combined to one new grid cell

With the standard deviation of the difference q, a threshold D with a confidence interval can be defined which states that all variables which are within the threshold are assumed as noise (Eq.19).

$$D = \pm \xi_{\alpha} \sigma_q \tag{19}$$

D = Threshold value
 ξ_{α} = Confidence interval (1.00 = 68%, 1.645 = 90%, 1.96 = 95%)

It is important to note that the confidence level can be propagated according to the desired level of detection. A low confidence level implies that – if a value lies outside the confidence interval – it is less sure that this value really is an actual change in the topography or if it still belongs to the noise.

2.5.6 Application in ArcGIS

The two elevation models need to have the same cell size so that it is possible to deal with the error propagation. The grid size was set to 2x2 meters which means that the LiDAR DEM from 2009 needed to be coarsened. This was done with the tool *Spatial Analyst Tools-Generalization-Aggregate* with a cell factor 2 and that it takes the mean of the four cells for the new cell.

Figure 18 shows the particularly created model which simplifies the calculations and shows the different steps.

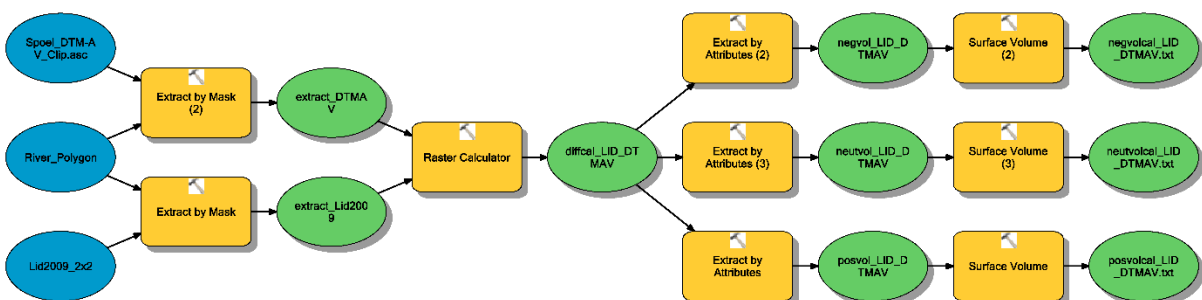


Figure 18: Custom model for DEM comparison in ArcGIS

In a first step (*Extract by Mask*), the two Elevation models were reduced to the spatial extent of the river. Two new raster files `extract_DTMAV` and `extract_Lid2009` are created.

The second step is carried out by the *Raster Calculator* which subtracts the newer (LiDAR) DEM from the older (DTMAV). A new raster file with the differences is created (`diffcal_LID_DTMAV`). Using the Tool *Extract by Attributes*, it is possible to extract values which lie in a certain range.

In this part, the error propagation comes into place. For all values which lie within the threshold value D it is uncertain if there is erosion or deposition. Those values are called "neutral" and they are added to the raster "`neutvol_LID_DTMAV`". The values which lie on the positive side or on the negative side of the threshold value are added to the rasters "`posvol_LID_DTMAV`" or "`negvol_LID_DTMAV`" respectively.

Using the command *Surface Volume* it is possible to sum up the elevation changes for each cell. This creates an estimate of the amount of deposited and eroded sediment in the river reach. When calculating the difference between the deposition and the erosion, an approximation of the sediment deficit over this time period can be quantified. It becomes therefore possible to create a sediment mass balance for the period between 2003 and 2009.

In a next step, the river polygon was cut into reaches between each cross section. With 113 cross sections, 114 reaches with a mean length of around 50 m were created. This step was done with the *Advanced Editing Toolbar* where the tool *Split Polygons* (symbol ) is able to cut a selected polygon with overlaying features. These features are in that case the cross sections created for the Basement 1D model.

Using the tool *Zonal-Zonal Statistics as Table*, it is possible to create statistics for each of the 114 reaches based on the "`diffcal_Lid2009_DTMAV`" raster. The result of this sequence of tools is a graph that shows the mean elevation change for each reach which can be used for the calibration of the 1D model.

2.6 Basement 1D Model

2.6.1 General Purpose

In a third part of the project work, a hydraulic model with sediment transport is created using the software Basement V2.3, which was developed by the Laboratory of Hydraulics, Hydrology and Glaciology (VAW) at ETH Zurich.

For the river Spöl, there are two publications on small scale sediment processes available (Mürle, 2000 and Noack, 2012) but the large scale sediment processes in this river are to this day largely unknown and have not been quantified. Therefore, to make first assumptions about erosion and deposition processes, a 1D (BASEchain) model was set up.

A 1D model is a simplification of the reality meaning that first, there is a uniform velocity in each cross-section and a uniform sediment distribution. There are no effects from curves which means the water elevation in the river does not lean towards the outer bank.

The hydraulic and sediment properties like the wetted area, the discharge Q or the shear stress τ are only computed at the cross section. This means, that the cross-sections have to be placed according to the structure of the river in order to see the effects of spatial irregularities.

2.6.2 Mathematical model

The in this case used module BASEchain is based on the Saint Venant Equations for unsteady, one-dimensional flow. This set of equations includes the mass balance and momentum conservation. The mass balance equation in a conservative form is defined in Equation 20.

$$\frac{\delta A}{\delta t} + \frac{\delta Q}{\delta x} - q_l = 0 \quad [20]$$

q_l = lateral discharge per meter of length [m^2/s]

The momentum equation is shown in Equation 21.

$$\frac{\delta Q}{\delta t} + \frac{\delta}{\delta x} \left(\frac{Q^2}{A} \right) - q_l u_x = -g \frac{\delta}{\delta x} (A \bar{h}) + gA(S_B - S_f) \quad [21]$$

u_x = flow velocity in x direction [m/s]

\bar{h} = water depth from surface to centroid [m]

S_B = Bottom slope [-]

S_f = Friction slope [-]

Those equations are governing the hydraulics of the river. The sediment dynamics are calculated using a one-dimensional bed load transport which consists of one single component for each grain size, the specific bed load flux in stream wise direction q_{Bg} . The equations are solved in order to obtain global bed material mass conservation. This uses the Exner-equation which adds up the masses of all sediment material layers between the bed surface and a reference level. This is done for all grain fractions and therefore directly results in the elevation change of the actual bed z_B (Equation 22).

$$(1 - \rho) \frac{\delta z_B}{\delta t} + \sum_{g=1}^{ng} \frac{\delta q_{B_g}}{\delta x} + \frac{\delta q_{B_g}}{\delta y} + s_g - sI_{B_g} = 0 \quad [22]$$

sI_{B_g} = source term per unit width, specifies a local input or output material (rock fall,...) [kg/m]

s_g = exchange per unit width between sediment and suspended material [kg/m]

The bedload transport rate q_{B_g} can be calculated with a variety of empirical approaches e.g. Meyer-Peter and Müller (1948), Parker (1990), Günter (1971), Rickenmann (1991) or Smart-Jäggi (1983). The approach used in this case study is by Wu Wang and Jia (2000) which shows similarities to the approach of Meyer-Peter and Müller but also includes the hiding-exposure mechanism for non-uniform transport (see Chapter 0 d.)).

The transport capacity Φ_{B_g} with the approach of Wu Wang and Jia is given by Equation 23.

$$\Phi_{B_g} = 0.0053 \left[\frac{\theta'}{\theta_{cr_g}} \right]^{2.2} \quad [23]$$

With the transport capacity obtained in Equation 22, the bed load transport rate can be calculated with Equation 24.

$$q_{b_g} = \beta_g \sqrt{(s - 1)gd_g^3} \Phi_{B_g} \quad [24]$$

β_g = volumetric fraction of grain size class g in active layer

2.6.3 Cross-section extraction

As a first step of the model construction, the different cross-sections have to be extracted from the available LiDAR DEM into the 1D grid editor in Basement.

a.) From DEM to HEC-RAS Geometry

To extract the cross-sections, the tool HEC-GeoRAS V10.1 from the US Army Corps of Engineers (USACE) was used, alongside with the ESRI ArcGIS 10.2 Desktop Suite. The interval of the cross-section was chosen to be 50 m because the structure of the river changes frequently and also the hillslope have different gradients. For the whole reach, a total of 113 cross sections were extracted. The width of each cross-section is set to 100 m.

Figure 19 shows the extracted cross-sections.

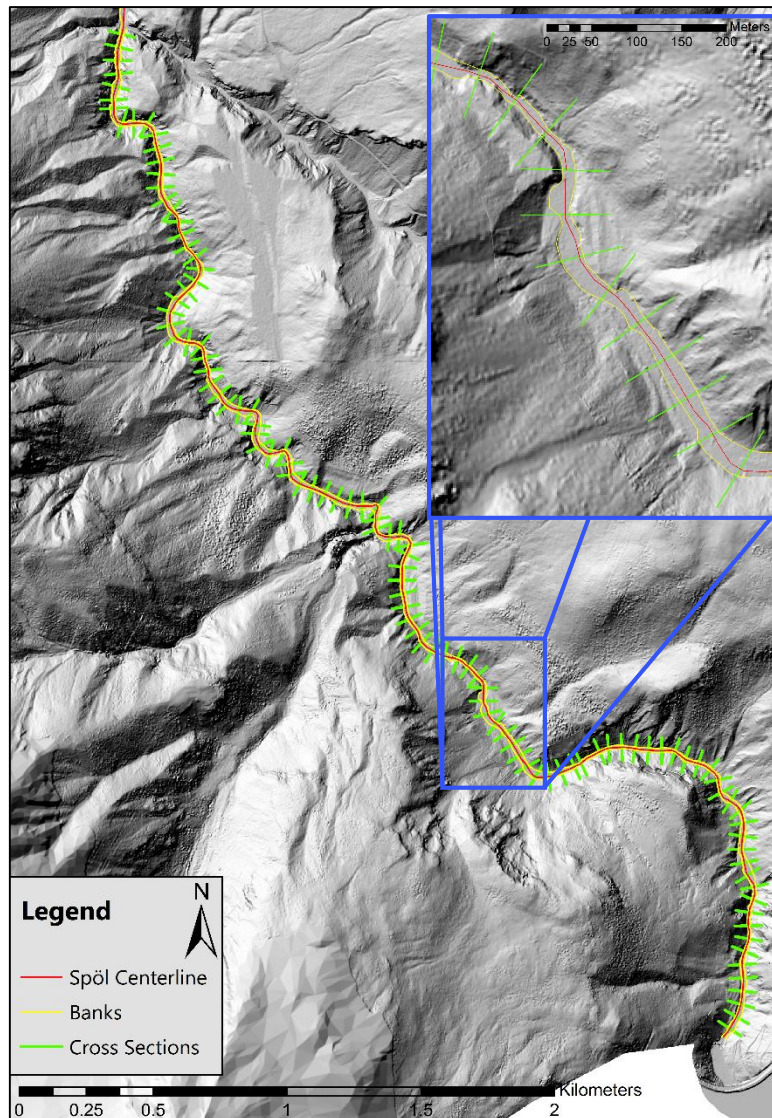


Figure 19: Cross sections extracted with HEC-GeoRAS

With the HEC-GeoRAS tool, also the roughness was extracted using a habitat map from the Swiss National Park (HABITALP map). The map shows different terrestrial habitat classes which can be used for a roughness classification. The roughness is assigned to the habitat class according to Table 5.

Table 5: Assigned roughness to habitat classes (PSW, D.R. Knauf)

Landuse type	k_{st} [$m^{1/3}/s$]
Water bodies	34
Swamps	40
Agriculture	40
Grass, meadow	40
Immature soil, extreme locations	35
Field shrubs	20
Forest	20
Supply and waste removal	70
Settlement, transportation	70

For the roughness of the river bed, the mean of the 42 line-by-number analysis samples was taken.

The "Water bodies" polygon did not match the manually created "River Polygon" which is described in Chapter 2.5.4. This circumstance had to be adjusted in a way that the HABITALP map was clipped with the River Polygon, the clipped fields were deleted and the River Polygon was merged with the HABITALP map.

b.) From HEC-RAS geometry to BASEMENT geometry

The roughness values which were taken from the HABITALP class gave multiple roughness values for the right and left overbank. The Python script, which transforms HEC-RAS geometry files (file extension *.g01) to BASEMENT geometry files however cannot handle multiple roughness values for each overbank. Therefore, they had to be reduced in the HEC-RAS geometry editor to a single right- and left overbank value.

c.) Basement geometry modifications

The geometry which is imported into the BASEchain geometry module has to be modified in various ways in order to perform smooth simulations. Figure 20 shows the effect that erosion or deposition has on the cross-section geometry.

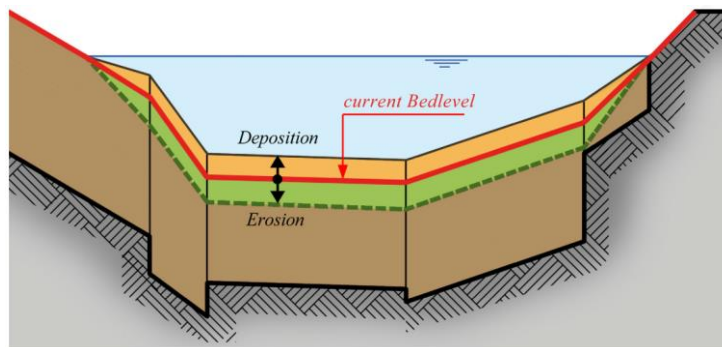


Figure 20: Effect of bed load on cross-section geometry (Laboratory of Hydraulics, Hydrology and Glaciology, 2013)

However, when more than just the nodes in Figure 20 are given due to the export from HEC-RAS, problems can occur when there are erosion and/or deposition processes. To generate the erosion or deposition triangle, BASEchain uses the next node on the left and on the right side of the bottom range definition. This effect is shown in Figure 21. When large erosion processes occur, the orange part grows and the water will not flow over the orange section but on its left and right side. Therefore, the deposited sediments won't be eroded again and the deposition grows to infinity.

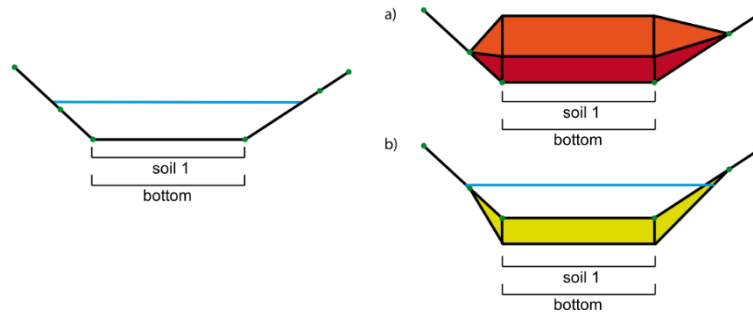


Figure 21: Deposition a) and erosion b) due to bedload with cross section points on embankments. (Laboratory of Hydraulics, Hydrology and Glaciology, 2013)

This problem can be solved with manually removing nodes on the left and of the right of the bottom range definition and with adjusting the bottom range to the edge of the flat part of the valley.

Figure 22 shows how the geometry in cross section 13 looked like when imported from HEC-RAS on the left, and on the right the same, manually modified cross-section.

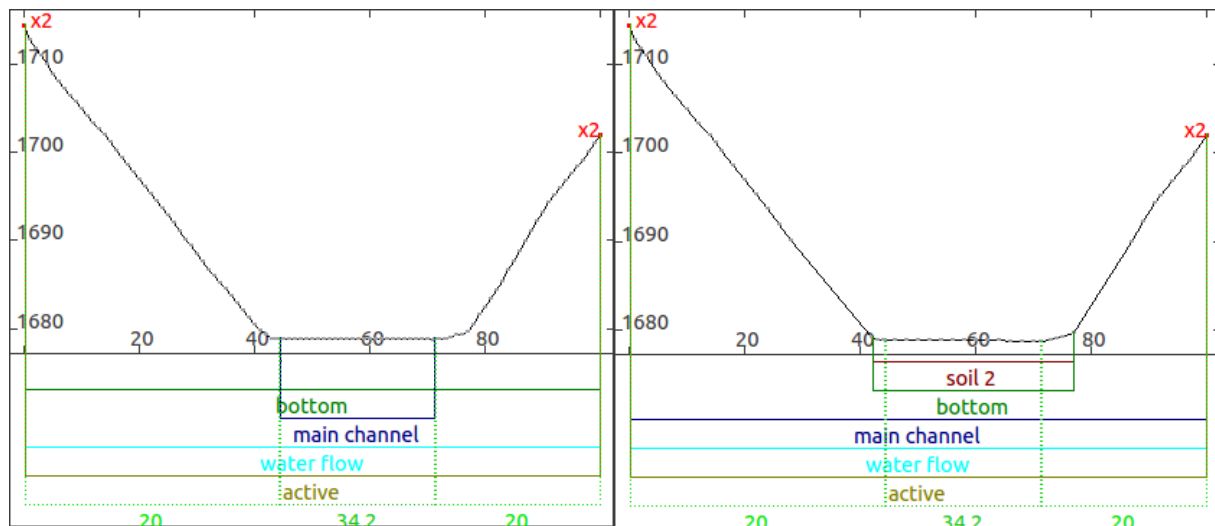


Figure 22: Raw (left) and modified (right) geometry of cross-section 13 (Basement)

First, the bottom range which is over the whole cross-section length has to be reduced to just the erodible soil part of the valley which is in this case from around 42 m to 78 m. Secondly, a soil definition parameter (in this case soil 2) has to be added. This defines the soil type of the ground with a grain size distribution that can be described in the BASEchain command file. The soil type has to have the same extent as the bottom range.

In a third step, the node network needs to be simplified. This can be done with the *Remove Nodes* tool with a threshold of 5 – 10 cm from the line. This step reduces the amount of manual removing of nodes significantly. As a fourth step, the nodes which lie close to the beginning or the end of the bottom range need to be removed for avoiding patterns described in Figure 21. The last step is to widen the main channel definition to the whole cross-section extent. A definition of the main channel range is only necessary when dealing with flood plains. In this case, the valley is quite narrow and no significant flood plains are available.

2.6.4 Calibration of the model

A model has numerous parameters which either are empirically estimated or physically based. The goal of calibration is to find the best parameter set which represents the natural processes best. For calibration, always a real measurement of a process has to be available which can be compared to the model results.

For this case study, there is no real measurement of any sediment processes available. However it is still possible to compare the results from the model with the DEM differences which give a general trend of the river behavior over time. The mean elevation changes which are used for calibration are described in Chapter 2.5.6.

The mean elevation changes per cross-section can also be obtained as an output file from the Basement simulation which makes a comparison between the two possible.

To quantify the quality of the model output, some goodness-of-fit measures can be used but also visual judgment is important.

The goodness-of-fit measures used in this case are:

Mass balance error

The mass balance error m [%] expresses the matching of the totals of both, the simulated and the observed elevation changes (Equation 25).

$$m = 100 * \frac{\sum_{i=1}^n (h_{sim,i} - h_i)}{\sum_{i=1}^n Q_i} \quad [25]$$

$h_{sim,i}$ = Simulated elevation change i

h_i = Observed elevation change i

Correlation coefficient

The correlation coefficient r (Eq. 26) expresses the linear dependence between the observed and the simulated elevation changes. The correlation coefficient lies between -1 and 1 where a higher positive value means a higher correlation and a lower negative value shows a trend towards inverse correlation.

$$r = \frac{\sum (x - \bar{x})(y - \bar{y})}{\sqrt{\sum (x - \bar{x})^2 (y - \bar{y})^2}} \quad [26]$$

x = observed elevation changes

\bar{x} = mean observed elevation change

y = simulated elevation changes

\bar{y} = mean simulated elevation change

Nash-Sutcliffe efficiency

This criterion measures how good the variability in the observations is explained by the simulations. It's one of the most commonly criteria used in hydrology (Eq. 27).

$$E = 1 - \frac{\sum_{i=1}^n (h_{sim,i} - h_i)^2}{\sum_{i=1}^n (h_i - \bar{h})^2} \quad [27]$$

$h_{sim,i}$ = Simulated elevation change i

h_i = Observed elevation change i

\bar{h} = mean observed elevation change

A perfect fit in terms of variability would be reached if $E = 1$. When the simulations would not show any variability, E would be 0. In between, there is a range which evaluates how good the model fits. They are listed in Table 6.

Table 6: Range of goodness for the Nash-Sutcliffe criterion

E	Fit
< 0.2	insufficient
0.2 – 0.4	satisfactory
0.4 – 0.6	good
0.6 – 0.8	very good
> 0.8	excellent

The calibration is carried out until the best possible parameter set is found which satisfies the goodness-of-fit measures the most.

The model is physically based which means that there are only a few parameters which can be calibrated. For a first test run, the model was configured running with a CFL-criterion of 0.95, with an initial time step of 3 s and a maximum time step of 250 s. The upstream boundary condition is a steady-state hydrograph with a defined slope of 1.5 %. This slope is extracted from the Centerline in ArcGIS. The downstream boundary condition is an internal h_q -relation which calculates the outflow due to the topography. The downstream slope again is extracted from the Centerline in ArcGIS and is set to 1.3 %. The initial hydraulic condition is a dry river bed and the minimal water depth in the bed is set to 0.06 m. The control volume thickness is set to 0.1 m.

With this configuration, a steady state run of 2 m³/s was run for a couple of days and the resulting hydraulic conditions at the end of the simulation (SpoelRestart.dat) were set to be the new initial hydraulic conditions instead of a dry river bed. Now, the river morphology block was added with a single grain bed material of 3.9 cm which corresponds to the d_m of the line-by-number analysis. As a bedload closure formula, the approach by Wu was selected. The upwind criterion is set to 1 and the θ_c is set to 0.05. The hiding-exponent by Wu et al. (2010) is set to -0.6 and the local slope criterion is set to off. The upstream bed material boundary condition is set as a constant sediment discharge rate of 0 m³/s because there is the dam Punt dal Gall. The downstream bed material boundary condition is set as IODown, where the same amount of incoming sediment from the upstream cross-section is released from the last downstream cross-section. The downstream boundary condition with the water level of the Ova Spin reservoir could not be applied because the last cross-section of the river reach lies higher than the highest elevation of the lake Ova Spin.

With this complete model, the first steady-state runs could be conducted and the reaction of the model to the mean bed elevation could be observed. In the first test runs, there were large oscillations throughout the river bed which caused the program to crash due to severe numerical errors. One way to solve this was to re-extract the whole geometry beginning in ArcGIS and via HEC-RAS to Basement, but this time in a finer resolution of 10 m instead of 50

m between each cross-section. The reason is that the finer the resolution, the better the results will be and therefore those numerical instabilities might disappear. However, the finer resolution with a total of 567 cross-sections did not bring the desired effect and the oscillations were still present. However the instabilities were caused by the geometry and not by the parameter set. Finally, the reason for the problems was, that the computational procedure described in Figure 21 for erosion and deposition had not been applied by then in the geometry. After applying the described steps in Chapter 2.6.3 c.), the model worked without numerical error messages.

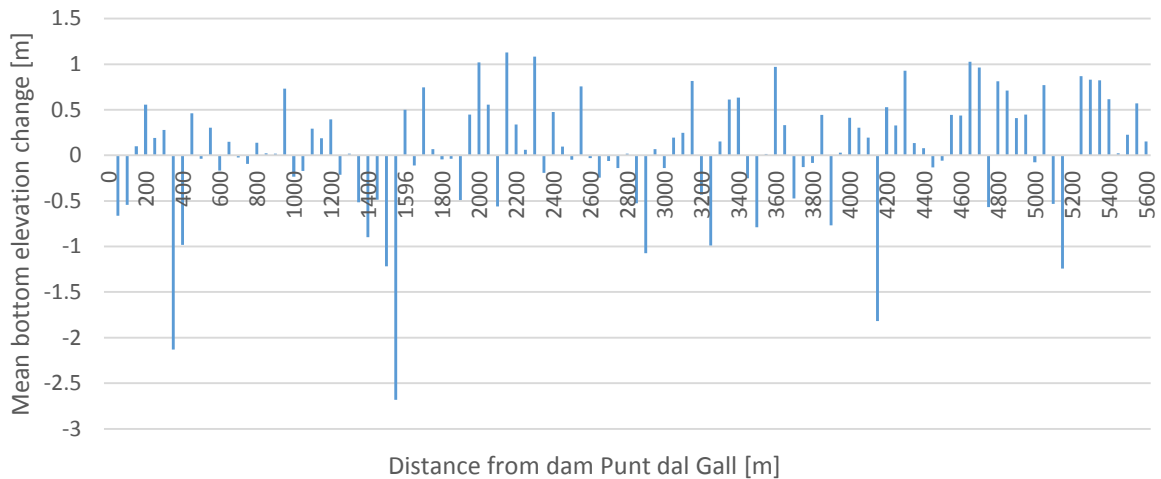


Figure 23: Steady-state run with 15 m³/s, single grain size, 2.3 days

The above shown Figure 23 shows an oscillating pattern for some cross-sections with altering erosion and deposition processes. For a flow of 15 m³/s there should not be such oscillating effects in a river. One common way to reduce the oscillations is to change the *upwind* factor from 1 to something between 0.5 and 1. This factor describes how the sediment transport over the edge of a cross-section is calculated. Having *upwind* set to 1 means that the transport of the upstream reach is taken for the transport over the edge of the cross-section. An *upwind* factor of 0.5 however weights the upstream and downstream transport with 0.5 and therefore balances the transport over the edge. The *upwind* factor should not necessarily be set too low because this would smear out the results over the whole length, however it was just for safety reason set to 0.5. It could later be increased until the model starts oscillating again.

Now, a multiple grain distribution could be added instead of a single grain distribution. For this, a representative line-by-number analysis sample (Sample 9B). The grain size distribution entered in the model consisted of the estimated d_{10} (0.2 cm), d_{30} (1.3 cm), d_{50} (3.9 cm), d_{70} (5.8 cm), d_{90} (11.1 cm), each as a fraction of 20%. With the multiple grain distribution, first also steady-state simulations were carried out with different discharges (2 m³/s, 5 m³/s, 10 m³/s, 20 m³/s) to see if there are any numerical problems with the sediment transport.

The simulations run fine, except in some cases, the grain fractions β_i in the control volume do not sum up to 1.0 resulting in a "sumofbeta" error. This problem is a bug in Basement and cannot be resolved for this study because it would need a lot of debugging work in the code. However with changing the control volume thickness from 0.1 to 1.15 m, the errors appeared less often.

For the transient case with the floods of the years 2003 - 2009, the 10 min flow hydrograph was cut to values that are above $1.5 \text{ m}^3/\text{s}$. It is assumed that below this discharge, no sediment transport occurs in the river bed. To cut the hydrograph, the function *aboveThresh* in MATLAB was used.

The 10 min hydrograph which would run for 469200 s (5.4 days) could not be used as hydrograph input file in Basement, most probably because there were too many rows. So the hydrograph was coarsened to show 20 min average values. Figure 44 in the Appendix shows the hydrograph. Now, the simulation was run for the whole period and compared to Figure 36. The goodness of fit between the mean elevation change and the DEM-differences were quantified using mass conservation, correlation and Nash-Sutcliffe coefficients (Chapter 2.6.4). The measures were taken once up to the "Droppoint" and once for the full extent. Goal of the calibration was primarily to increase the goodness-of-fit criteria and secondarily not having "sumofbeta" errors. With those limitations, the parameters θ_{cr} , the hiding-exponent, the local slope (on or off), the bedload factor (which increases the bedload by a factor) and finally the upwind factor were calibrated.

2.6.5 Validation of the model

In model validation, the model performance is analyzed using e.g. a different period of the time-series input. Here, the previously defined parameter set is checked to see if it is robust. In this case study there is no data available for a validation of the model. Therefore this step cannot be performed.

2.6.6 Modelling tasks

The aim of the sediment model is to find out when and at what discharge is the initiation of motion in the river reach. To find this out, some steady-state simulations are carried out over a longer period of time. This will also answer the question whether the system stable during the low-flow periods.

With the calibrated model it was possible to run steady-state simulations for one week with different discharges ($1 \text{ m}^3/\text{s}$, $1.5 \text{ m}^3/\text{s}$, $2 \text{ m}^3/\text{s}$, $5 \text{ m}^3/\text{s}$, $10 \text{ m}^3/\text{s}$, $20 \text{ m}^3/\text{s}$, $30 \text{ m}^3/\text{s}$, $50 \text{ m}^3/\text{s}$, $100 \text{ m}^3/\text{s}$) to see up to which discharge the bed is stable and where the general dynamic processes start.

Furthermore, it would be interesting, how much sediment is washed out for a flood event. The second part of the simulation included transient flood wave runs with simplified, synthetic flood events. According to Table 2, the floods should be released for 6 to 9 hours and they should be between 10 and $30 \text{ m}^3/\text{s}$. However, the time series showed that the largest flood had a maximum discharge of over $75 \text{ m}^3/\text{s}$ (03.07.2013). Therefore, floods with a peak flow from 10 to $65 \text{ m}^3/\text{s}$ were simulated. Floods with a higher peak caused the model to crash, mainly due to the simplified shape of the hydrograph. Figure 24 shows the simplified floods that were used as an upstream hydrograph in the model. After the flood, the model ran for another 19.4 hours in order to reach steady-state conditions again.

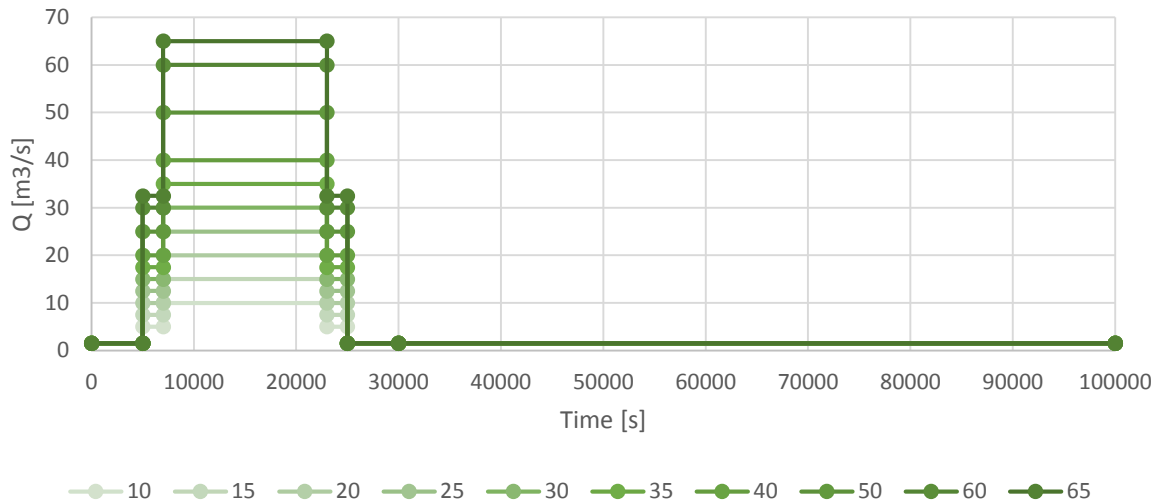


Figure 24: Synthetic floods with different peaks for a duration of 30000 s (8.3 hours) and low flow of 70000 s (19.4 hours)

With the transient case simulations it was possible to estimate the amount of sediment that is flushed out of the system for each flood at various points. For this case, two points were chosen. The first point is cross-section 81, which is the last cross-section before the "Droppoint". This cross-section also stands for the end of the reach where mostly erosion occurs and therefore the highest amount of sediment is transported through this cross-section. The second point of observation is the last cross-section (CS 113), which shows how much sediment leaves the observed reach in total at the place where the river Ova il Fuorn joins the Spöl. This amount of sediment will later on be deposited in the reservoir Ova Spin, giving therefore an important estimate on the amount of aggradation that is observable per flood.

3 Results

3.1 Line-by-number analysis

Figure 25 shows an overview of the obtained values for each sample in a longitudinal profile.

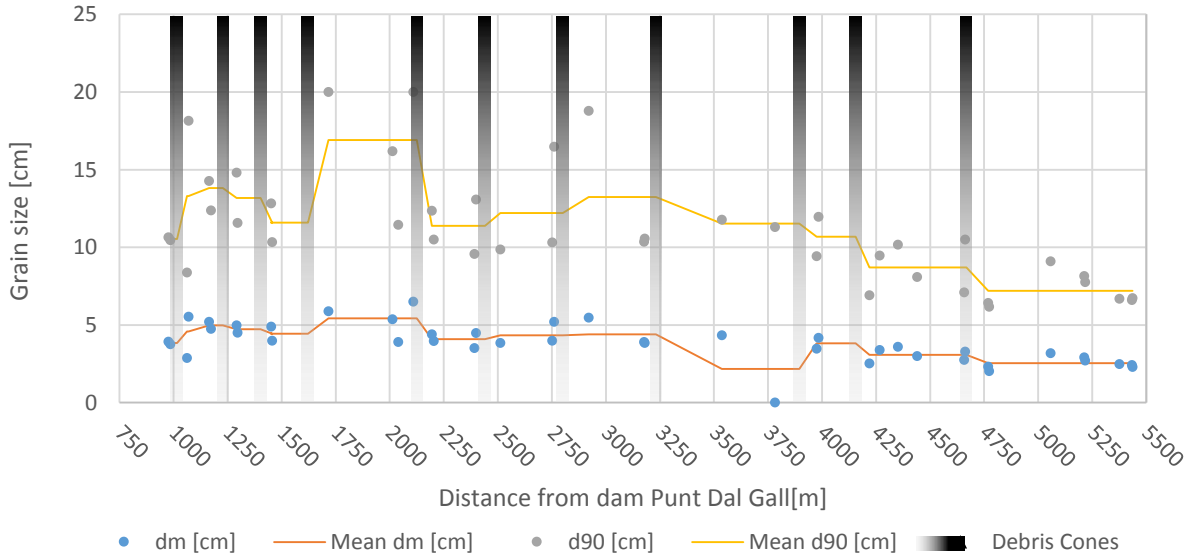


Figure 25: Overview of the line-by-number analysis samples across the river reach. The points describe the sample values obtained and the lines describe the mean value from the first sample after a debris cone up to the next cone. The cones are indicated as a gradient line.

Figure 25 shows on one hand the determined sample values for the d_m and d_{90} but also a mean value which was calculated between each debris cone. It can be seen that after each debris cone, the grain size distribution is altered and then stays the same up to the next cone. This shows, that the grain size distribution is influenced by lateral inputs such as debris cones.

The relative changes of the grain size diameter at each debris cone are shown in Table 7.

Table 7: Relative change of the grain size diameter at each debris cone

Debris Cone	Change [%]
1	19.2
2	-6.3
3	-7.7
4	25.2
5	-34.2
6	6.5
7	1.4
8	-8.6
9	-6.2
10	-18.9
11	-14.0

Table 7 above shows that the d_m at seven of eleven debris cones decreased. The maximum decrease was measured at debris cone 5. In four of eleven cases, the d_m increased with a maximum of 25.2% at the debris cone 4.

Furthermore, it was possible to acquire a grain size distribution equally to Figure 9. Some of the line-by-number analysis points were specifically taken at a side-arm where an armoring layer was present and on a moving bedload bar. Figure 26 shows the corrected and transformed grain size distribution plotted with their weight fractions q_i against the grain size diameter.

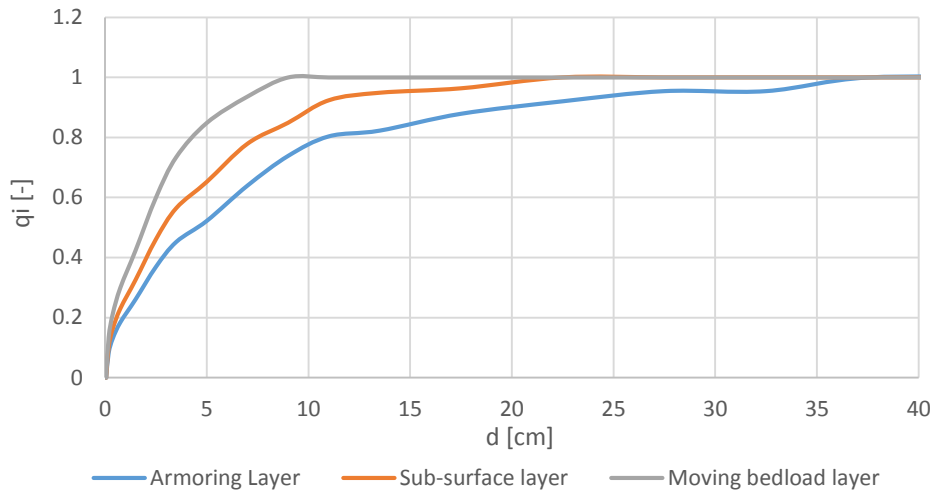


Figure 26: Grain size distribution variations depending on layer type, shown as a weight fraction q_i [-]. The layers described are taken from specific sample distributions observed in the field.

Figure 26 shows the armoring layer with higher amounts of coarse grains than the sub-surface layer whereas the moving bedload layer shows the smallest amount of coarse grains.

Table 8 shows the basic statistics of the d_m and the d_{90} of the sub-surface layer respectively.

Table 8: Basic statistics of the line-by-number analysis with the mean grain diameter d_m and the characteristic diameter d_{90} for the sub-surface layer.

	d_m	d_{90}
Mean [cm]	3.9	11.1
Std Dev [cm]	1.1	3.6
Skewness	0.3	1.0
Kurtosis	-0.4	0.4
Min. [cm]	2.0	6.2
Max. [cm]	6.5	20.0

Figure 27 shows the plotted slope versus the d_m of each sample.

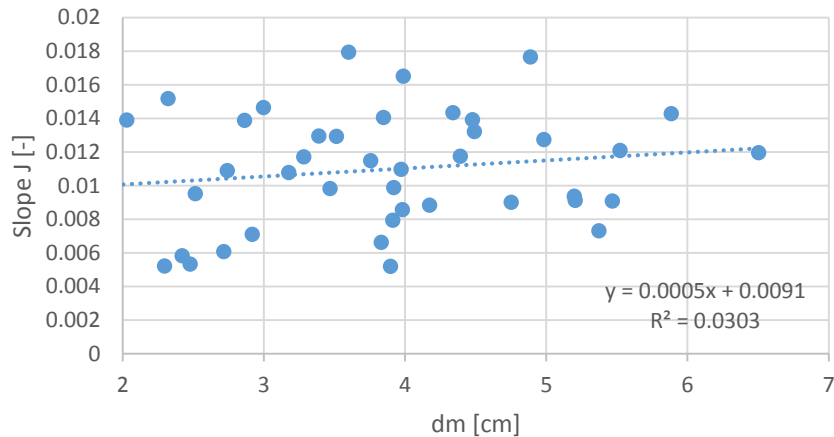


Figure 27: Relationship between mean grain diameter d_m and slope J

As it can be seen in Figure 27, there is no statistically significant trend observable between the mean diameter and the slope. Generally there is a slight increase of the grain size diameter when having a higher slope.

The roughness of the river reach is expressed with the k_{st} . The histogram of the 42 calculated k_{st} values is shown in Figure 28.

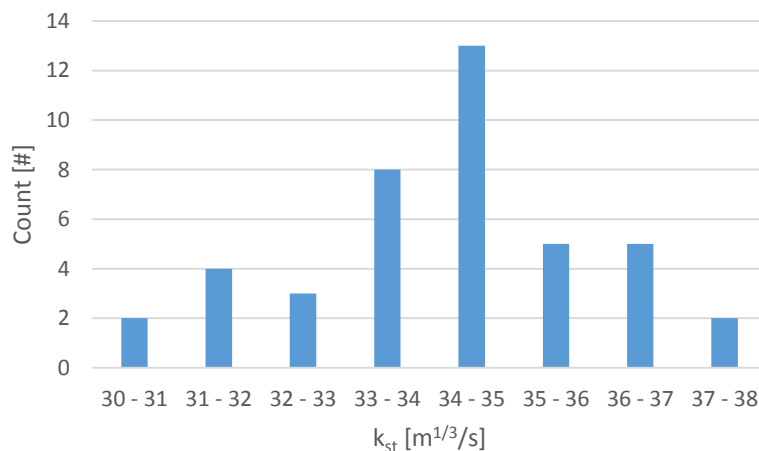


Figure 28: Histogram of k_{st} values for the reach in the Spöl

It can be seen that a k_{st} of 34 - 35 $m^{1/3}/s$ was the most observed value. This coincides with the determined mean value of 34.2 $m^{1/3}/s$. This mean value will be used for further calculations using Basement.

Additionally, the sample values were extrapolated to represent the roughness in the whole river reach. Figure 29 shows the general shift of the roughness using the kriging approach.

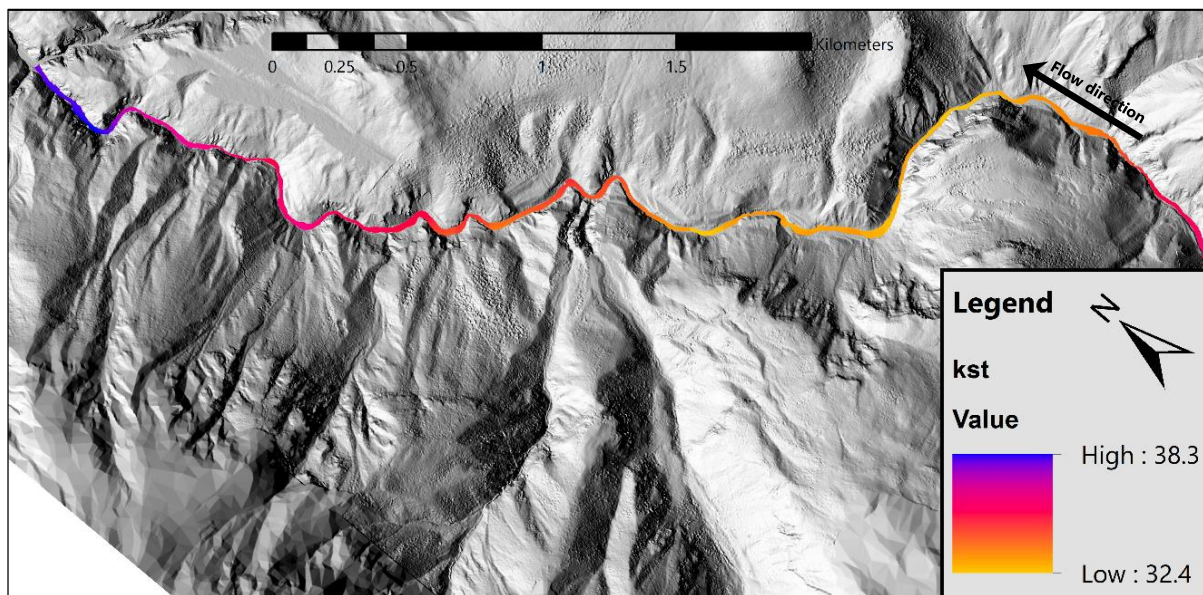


Figure 29: Kriging interpolation of river reach. (Maps: LiDAR 2009 © bfs swissphoto, DTM-AV © swisstopo)

The interpolation shows a medium to high roughness coefficient at the beginning of the reach. After the first left-curve of the river, a canyon-like part of the river begins with rather low roughness coefficients. Below the canyon, the roughness gradually increases until the end of the reach where the roughness is close to $40 \text{ m}^{1/3}/\text{s}$. The high roughness coefficients at the beginning of the reach only consist of calculated values because there was no sample taken at the uppermost part of the reach. The kriging interpolation does not have any values to create a variogram in this reach.

3.2 Results from DEM Comparison

3.2.1 DEM Properties

In order to quantify the difference to the elevation that an increase of the flow can have to the river bed, a steady-state simulation with the calibrated Basement model and a discharge of $20 \text{ m}^3/\text{s}$ was carried out. The mean increase of the water depth of the simulation was around 0.46 m with a standard deviation of 0.14 m . However, an artificial flood also leads to sediment dynamics in the river and to erosion and deposition processes which also can have an effect to the absolute elevation measured by the LiDAR 2009. Figure 15 shows that the flood already started 24 hours before the LiDAR survey. The flood was used as an input in a transient-case, bed load transport simulation and the mean water surface elevation change during the survey time was around 0.40 m with a standard deviation of 0.54 m .

3.2.2 Thalweg

As a first step to find erosion or deposition tendencies, the Thalweg from various available Digital Elevation Models was extracted. Figure 30 shows the Thalwegs for the elevation models from 2003 (DTM-AV) and 2009 (LiDAR).

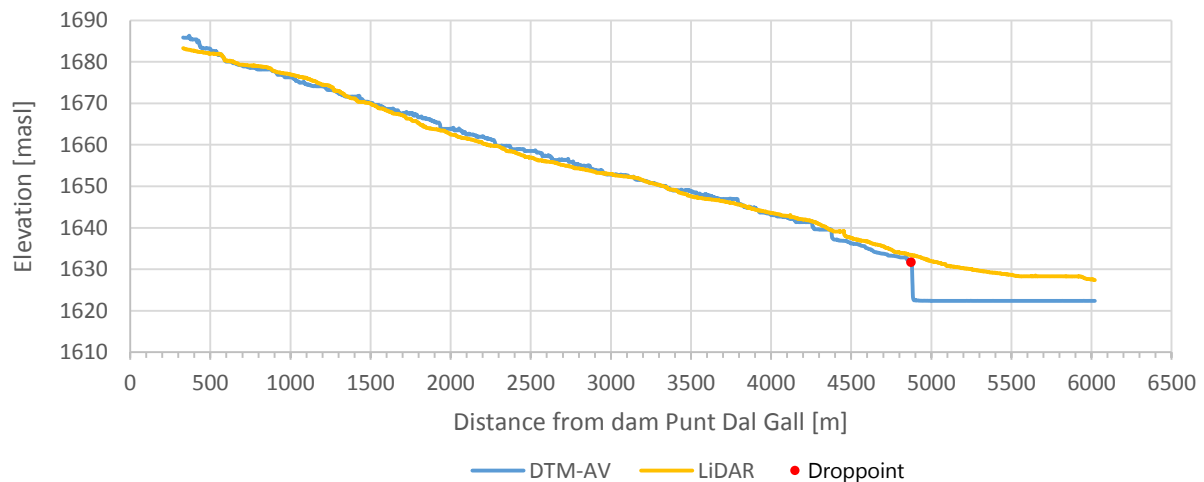


Figure 30: Different Thalwegs extracted from the DEMs DTM-AV (2003) and LiDAR (2009). The “Droppoint” shows a point where the DTM-AV drops around 10 m and stays constant from this point on.

At the beginning of the reach, just after the dam Punt dal Gall, there is an erosion tendency observable until around 600 m below the dam. From there on until 1400 m, there is no clear pattern visible as both lines lie close to each other. From 1400 m down to around 3300 m, the LiDAR 2009 Thalweg lies below the DTM-AV which shows a section of erosion. From 3300 m to around 4900 m, there is again no clear trend visible. At the distance of 4880 m below the dam, the DTM-AV shows a drop of around 10 m. This point – called “Droppoint” from here on – lies on the same point where on Figure 43 in the Appendix it is shown that the DEM flights were acquired on different times. For further analysis, this fact has to be included because it can be a major source of uncertainty in the analysis. The results will be evaluated once up to the “Droppoint” and once on the full extent where appropriate.

3.2.3 Erosion/Deposition pattern

A more advanced step in analyzing the sedimentation was a 2D analysis of the erosion or deposition patterns. For the analysis, an error propagation calculation had to be done first (see Chapter 2.5.5).

With a standard deviation of 0.06 m for the LiDAR 2009 dataset, the coarsened standard deviation (from 1 m grid to 2 m grid) could be calculated using Equation 18. The new standard deviation σ_{new} equals 0.12 m. With this, the standard deviation of the difference q could be calculated (with $\sigma_{\text{DTMAV}} = 0.5$ m) and resulted as $\sigma_q = 0.514$ m. A 90% confidence interval resulted in the Threshold value D of ± 0.85 m.

The following Figure 31 shows the three raster datasets “negvol_LID_DTMAV”, “neutvol_LID_DTMAV” and “posvol_LID_DTMAV” from Figure 18 (Chapter 2.5.6), each given a separate color.

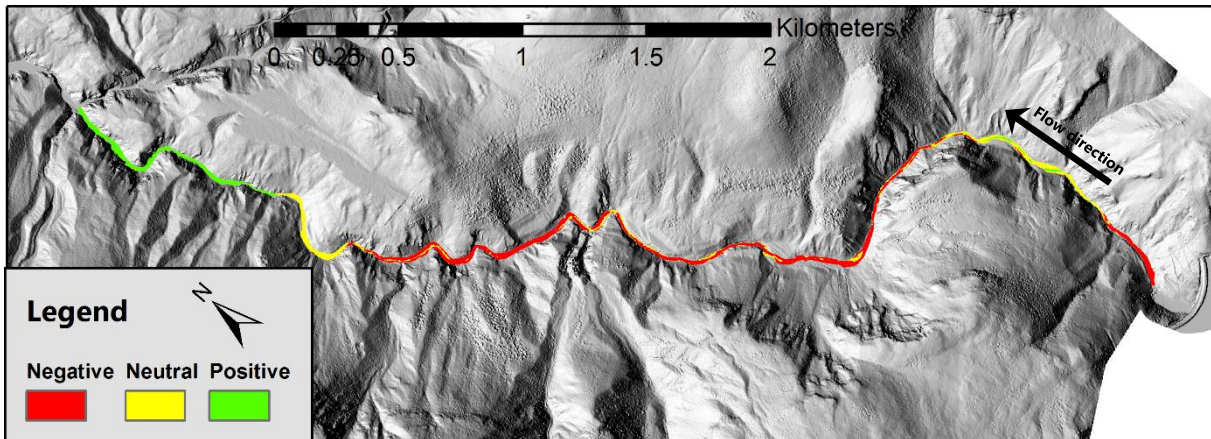


Figure 31: Negative, neutral and positive elevation changes for the river reach Spöl (Maps: LiDAR 2009 © bfs swissphoto, DTM-AV © Swisstopo)

In the Figure 31 above, the erosion and deposition patterns were not clearly visible, therefore two close-ups were made. Figure 32 shows the upper part of the regime, Figure 33 a section in the middle part of the reach and Figure 34 the bottom part of the river reach.

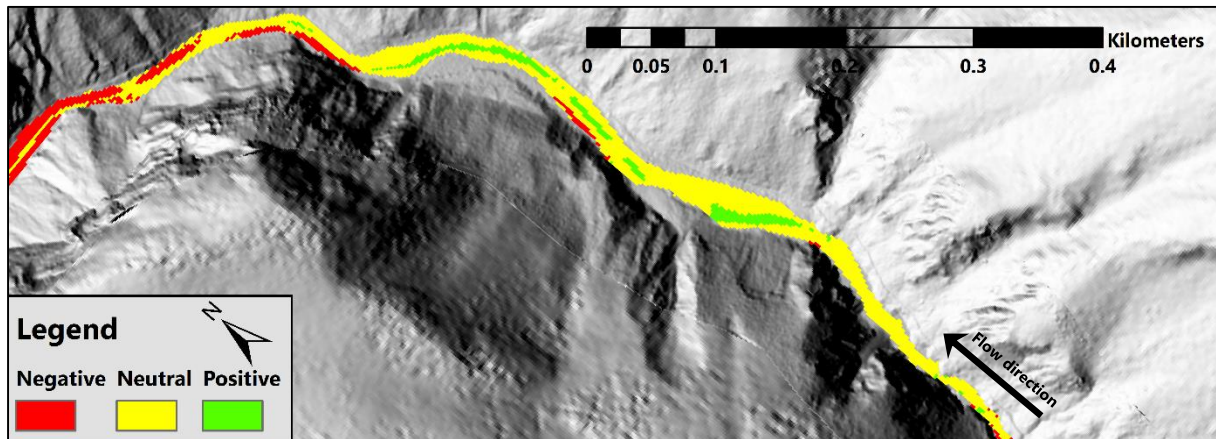


Figure 32: Upper part of the reach with deposition (positive, marked green) in the middle of the channel (Maps: LiDAR 2009 © bfs swissphoto, DTM-AV © Swisstopo)

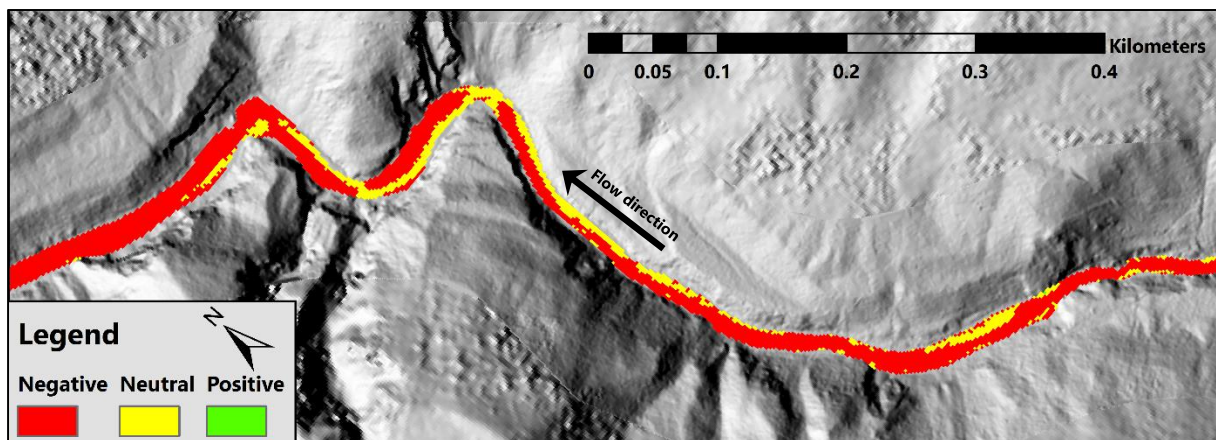


Figure 33: Middle part of the reach with largely erosion (negative, marked red) and some uncertain (neutral, marked yellow) zones at the banks (Maps: LiDAR 2009 © bfs swissphoto, DTM-AV © Swisstopo)

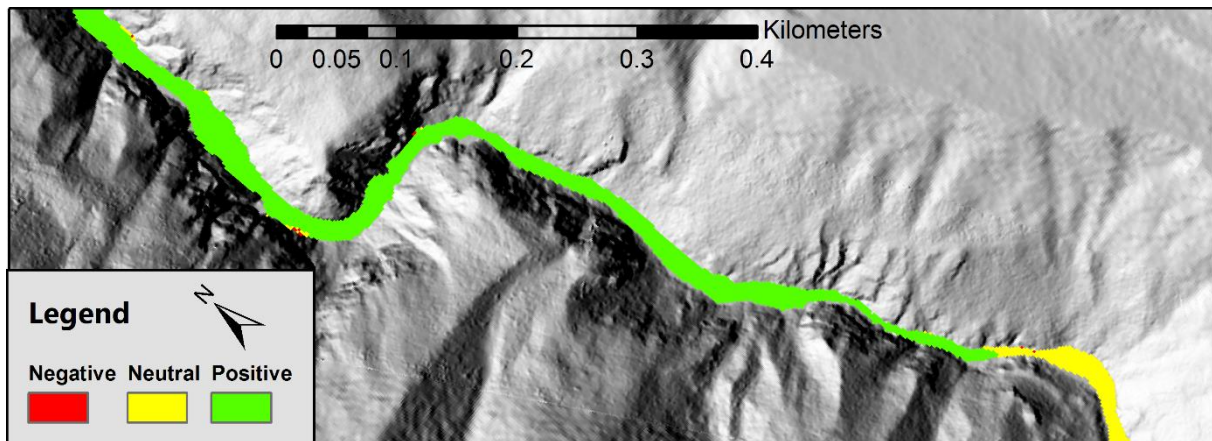


Figure 34: Lowermost part of the reach with mostly deposition (positive, marked green) and some uncertain zones (neutral, marked yellow) at the banks (Maps: LiDAR 2009 © bfs swissphoto, DTM-AV © Swisstopo)

The close-ups showed that the patterns of positive (deposition) or negative (erosion) values were not fuzzy distributed over the area but they show longer effects which look like gravel bars. The sudden change from neutral to positive in Figure 34 lied exactly at the same place where the “Droppoint” was observed in Figure 30. This shows that the drop in the DTM-AV was not only observable at the lowest points (Thalweg) but also over the whole river bed.

The first and uppermost part of the Spöl was dominated by erosion, followed by a reach that was mostly in the uncertain/neutral zone meaning that there are only small elevation changes. Figure 32 showed an interesting pattern with depositions in the middle of the river bed implying that gravel bars are more and more developed in the middle of the stream. The values were often more negative right at the river banks compared to values within the river, showing that they were more undermined by flow which results in erosion. In the lower part (Figure 33) there is an inverse trend, meaning that the middle of the river bed was eroded more than the banks. This could result from the steeper slope which results in a higher flow velocity in the middle of the river bed.

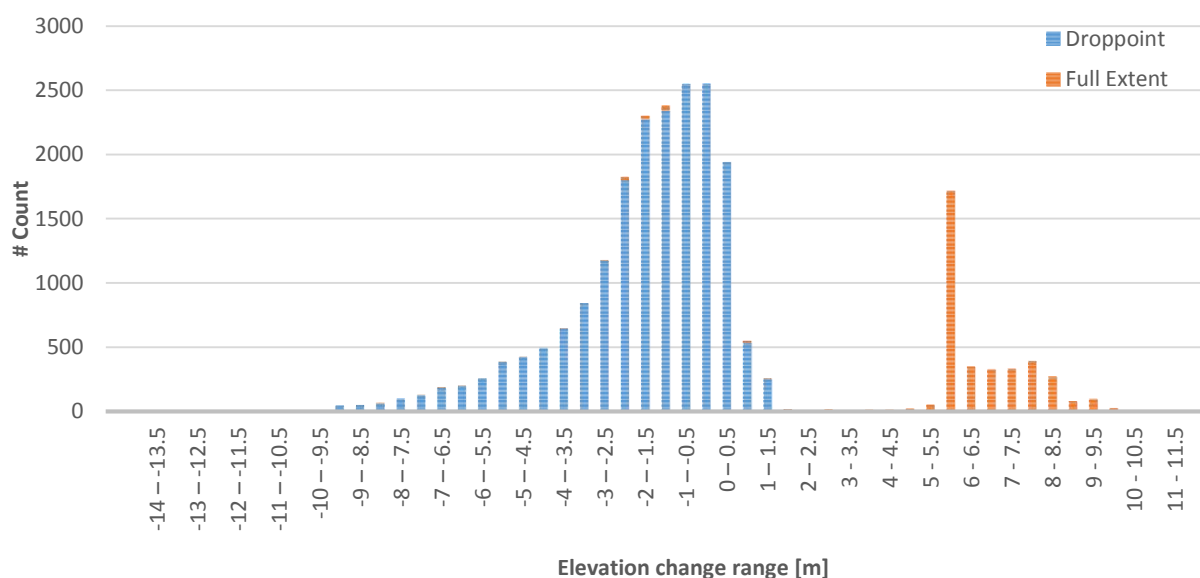


Figure 35: Histogram of the differences between LiDAR 2009 and DTM-AV up to the Droppoint (blue bars) and additional orange bars when looking at the full extent.

Figure 33 shows the histogram of the cell values up to the "Droppoint" (blue). It shows a highly skewed distribution with a slightly negative peak. When the histogram of the values is applied on the full extent of the reach, the "Full Extent" values (orange) are added to the distribution. They show a second distribution at highly positive elevation changes. There is a highly visible peak of this additional distribution in the range of 5.5 - 6 m.

The basic statistics of the "diffcal_LID09_DTMAV" raster are shown in Table 9, again, once up to the "Droppoint" and once for the full extent.

Table 9: Basic statistics of the differences between LiDAR 2009 and the DTM-AV up to the "Droppoint" and for the full extent.

	Extent up to "Droppoint"	Full Extent
Mean [m]	-1.78	-0.42
Std Dev [m]	1.94	3.60
Skewness [-]	-1.42	0.80
Kurtosis [-]	2.84	0.70
Max [m]	2.17	11.77
Min [m]	-14.21	-14.76

The mean elevation change up to the "Droppoint" was with -1.78 m much higher than the one including the rest of the reach (Table 9). On the full extent, the standard deviation also was higher. The skewness and kurtosis were heavily influenced by the second distribution.

The following Figure 36 shows that in most reaches, an erosion pattern can be observed which is larger than one meter. For the major part of the stream (from 1400 m below the dam up to around 4300 m), even the maximum value observed in the reach is negative. In the last part of the reach, there is clearly a deposition pattern. In this part (from 4880 m below the dam to the end), the minimum values are also positive.

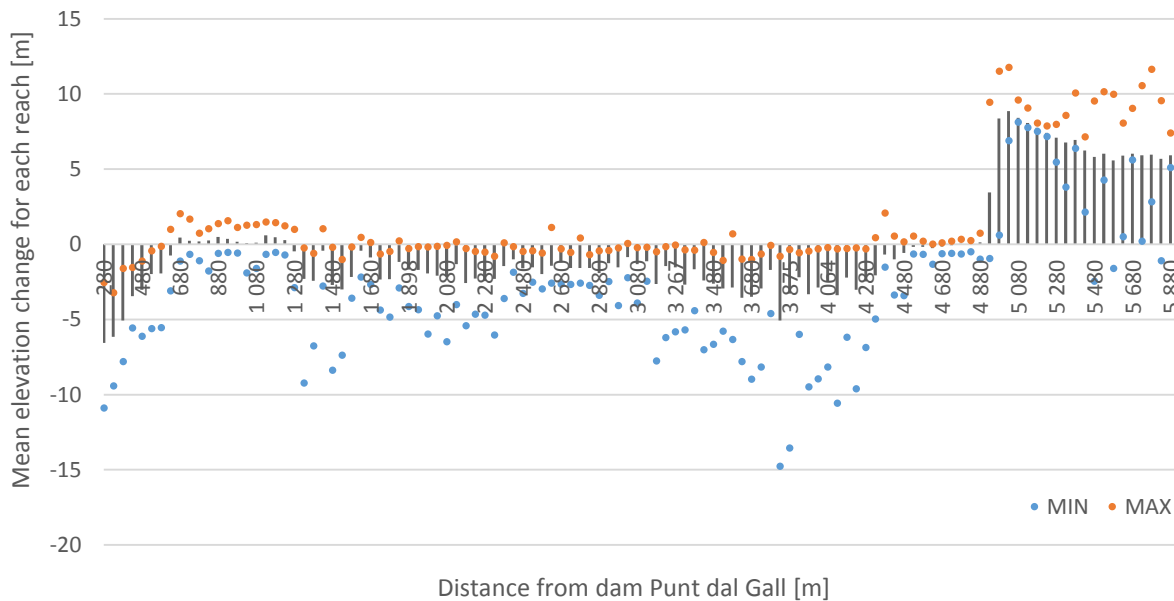


Figure 36: Mean elevation change for the full extent with min. and max. for each reach in the river Spöl

For the above Figure 36 it is important to point out that the “Droppoint” lies in the reach at 4880 m which is the first reach showing positive values after a long period of negative values.

3.2.4 Mass balance

The results of the covered area showed that the partial extent which only reaches the “Droppoint” is missing mainly positive values whereas the uncertain and negative values stay more or less the same (Table 10). The volumes in the negative part stay the same for both extents whereas the positive volumes are reduced by a factor of 100.

Table 10: Covered Area (how many cells are defined as uncertain, negative or positive) and sum of volume in m^3 for each class calculated for the full extent and up to the “Droppoint”.

	Covered Area [m^2]	Volume [m^3]
Full extent		
Uncertain	16636	-
Positive	13192	83133
Negative	37124	109980
Extent up to “Droppoint”		
Uncertain	16912	-
Positive	688	830
Negative	36844	109384

The Uncertain volume changes could not be calculated because the ArcGIS tool can only calculate values above or below a reference plane and not both. The “Uncertain” raster included negative and positive values.

The mass balance for both extents show a net-negative number which is an evidence of erosion along the reach. The balances are given in Equation 28.

$$\begin{aligned}
 \text{Netto Balance} &= \text{Positive volume} - \text{Negative volume} && [28] \\
 \text{Full Extent:} & 83133 \text{ m}^3 - 109980 \text{ m}^3 = -26847 \text{ m}^3 \\
 \text{Droppoint:} & 830 \text{ m}^3 - 109384 \text{ m}^3 = -108554 \text{ m}^3
 \end{aligned}$$

3.3 Basement 1D Model

The final parameter set consisted of a θ_{cr} of 0.045, a hiding exponent of -0.6, a bedload factor of 1.8, the local slope is enabled and the upwind factor was set to 0.5. The final calibration result is shown in Figure 37, the Basement calibration code is given in Appendix Chapter 6.1.

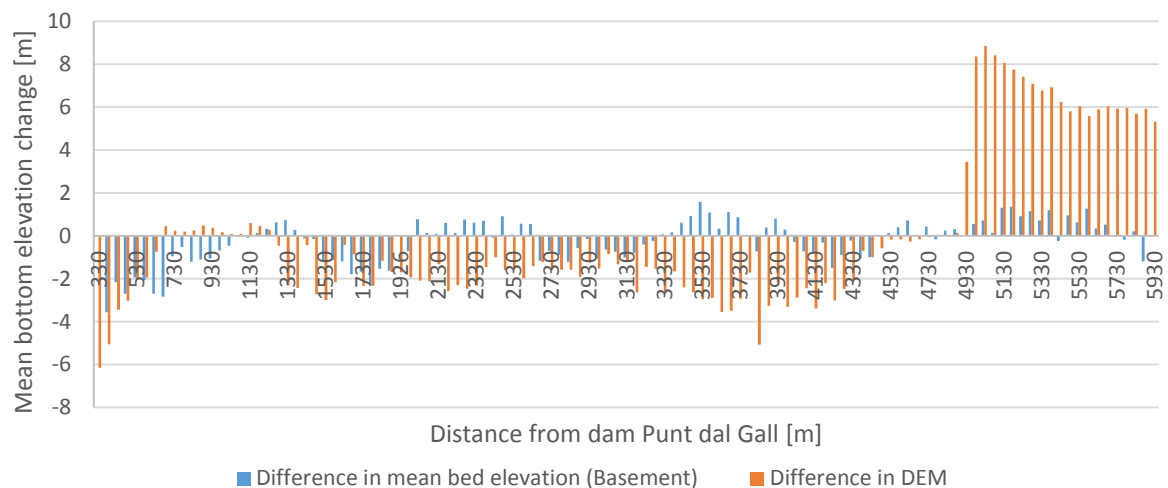


Figure 37: Final calibration run with all floods between 2003 and 2009 compared to the DEM-Differences for the full extent.

As it can be seen, the calibrated elevation changes did not fit the estimated elevation changes from the DEM very well. However, some general trends were visible like an erosion pattern at the beginning of the reach up to around 1000 m. Then, there was a short period of equilibrium to around 1300 m. After this point, both, the model and the DEM difference showed an erosion pattern whereas the DEM difference showed consistent erosion up to around 4500 m whereas the model did also show some reaches with deposition. From 4500 m below the dam to around 4900 m the reaches were again in both cases in an equilibrium. From 4900 m onwards both elevation changes show a consistent deposition until the end of the reach whereas the model did not show such high deposition values like the DEM differences did.

The goodness of fit measures before and after calibration are given in Table 11.

Table 11: Goodness of fit criteria and volume change for the calibration of the 1D model up to the "Drop point" and for the full extent

Criteria	Before calibration	After calibration
Up to "Drop point"		
Mass balance error [%]	-88.30	-75.57
Correlation coefficient [-]	-0.01	-0.08
Nash-Sutcliffe coefficient [-]	-1.88	-1.84
Full Extent		
Mass balance error [%]	1.25	102.73
Correlation coefficient [-]	0.21	0.34
Nash-Sutcliffe coefficient [-]	0.02	0.09

The criteria for the "Drop point" case did not lie in a range that could be considered as sufficient. The mass balance error could be improved from -88.30% to -75.57% but the changes for the other criteria are insignificant.

However, on the full extent, the mass balance error criteria was already well before calibration (1.25%). Due to the fact that there is the drop in the elevation model, this criterion is not the most important one so the goal was to optimize the other criterions without respect to the mass balance error. The correlation coefficient was positive and could be improved to 0.34

from 0.21. Also the Nash-Sutcliffe coefficient could be improved to 0.09 which is still in the range "insufficient". A sufficient Nash-Sutcliffe would be above 0.2.

3.3.1 Steady-State runs

Figure 38 shows the results averaged per day of these simulations.

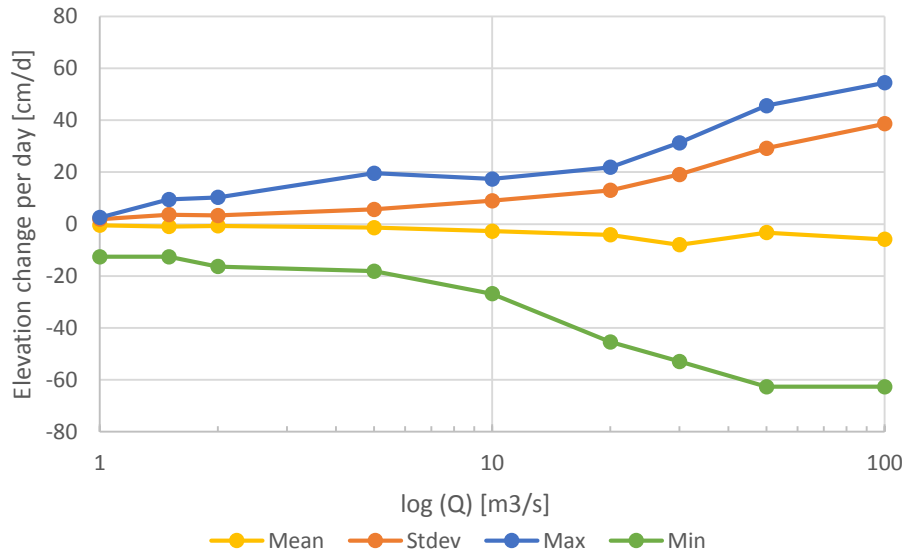


Figure 38: Mean elevation change per day and basic statistics over the whole reach for steady-state flow for the full extent.

The mean elevation change per day stayed close to zero up to a discharge of around 2 m³/s. For higher discharges, the mean became a negative value which means a couple of centimeters erosion per day. The maximum and minimum values of the elevation change increased with the discharge, so did the standard deviation. The skewness and kurtosis of the values are shown in the Appendix (Figure 45).

3.3.2 Transient runs

Similar to the steady-state runs, the mean elevation change of the river bed is evaluated with the different flood peaks (Figure 39).

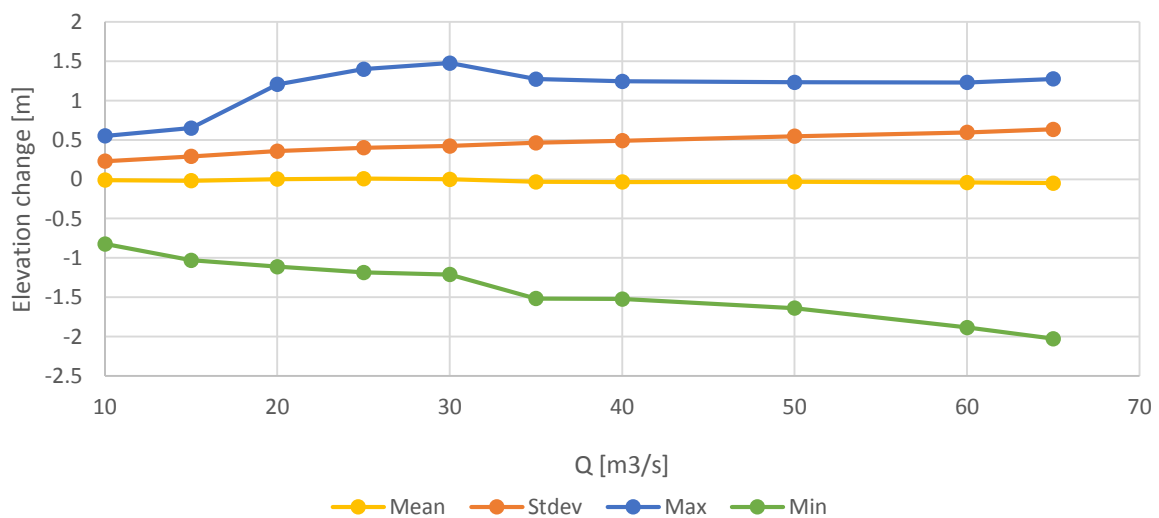


Figure 39: Mean elevation changes for each flood and basic statistics

The mean elevation change remained for all floods very close to zero whereas the maximum and minimum value increased resp. decreased a lot up to $30 \text{ m}^3/\text{s}$. The standard deviation of the values is at the beginning ($10 \text{ m}^3/\text{s}$) around 23 cm and increases to 63 cm for a $65 \text{ m}^3/\text{s}$ flood. The skewness and kurtosis of the values are shown in the Appendix (Figure 46).

The total bed load transport for various floods is shown in Figure 40.

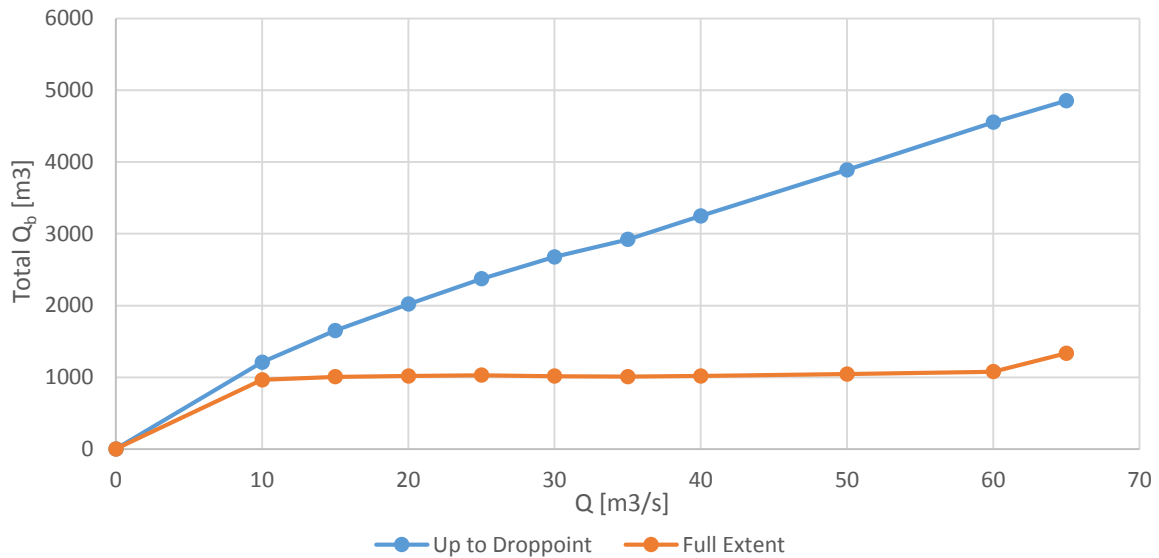


Figure 40: Total bed load transport (Q_b) for various flood events once to the "Droppoint" and once for the full extent.

The total bed load transport steadily increased at the "Droppoint" (CS 81) whereas it remained on a low level at the end of the observed reach (Full extent, CS 113). This showed that in the last part of the reach between cross-section 81 and 113, there is a lot of deposition happening which reaches a threshold at around $60 \text{ m}^3/\text{s}$. At this point the curve of the total bed load transport at cross-section 113 starts increasing with a similar slope like cross-section 81 at the "Droppoint".

4 Discussion

4.1 Line-by-number analysis

The line-by-number analysis proved itself to be a simple tool to gather a large amount of data in a small amount of time. When looking at the resulting mean grain size (d_m) of 3.9 cm, it matches well with a previous, more advanced assessment using freeze-coring which is widely accepted to be the most accurate method to take sediment samples in rivers. With this method, Noack (Noack, 2012) determined the d_m of the sub-surface layer to be 3.4 cm.

The presented basic statistics in Table 8, showed good results with a reasonable standard deviation (1.1 cm with line-by-number analysis compared to 0.85 cm with freeze-coring (Noack, 2012)). However the calculated d_{90} of 11.1 cm is slightly higher than the results from Noack (2012), who calculated a d_{90} for the sub-surface layer of 8.24 cm.

Comparing the calculated k_{st} value of $34.2 \text{ m}^{1/3}/\text{s}$ with the literature, this value describes a river with a natural bed with head-sized scree material and with medium to high sediment-bearing. In such rivers, also vegetation such as weeds or algae in the river bed can have an influence on roughness, compared to a pure mountain stream where no vegetation can grow in a river bed.

The histogram of the extracted k_{st} values (Figure 28) showed a distribution from $30 \text{ m}^{1/3}/\text{s}$ to $40 \text{ m}^{1/3}/\text{s}$ which means that the channel is not uniform along the reach. This can also be seen in Figure 29 which shows the spatial evolution of the k_{st} values.

In the majority of debris cones (seven of eleven) the mean grain diameter decreased up to 35%. Following from those values, the debris cones bring more fine material into the river system than coarse grains and blocks.

During a flood, the water in the channel rises up to the level where the large deposits at the bottom of the debris cones are situated and the present shear stress manages to move many of those grains downstream. Due to the fact that the floods are only of a short period (6 - 9 hours), the coarser grains will not be transported a long way because during the low flow periods, the shear stress is not high enough to move them any further. The fine particles however can also be moved during the low flow periods which – after a flood – steadily build up a new armoring layer in the river bed. This description would imply that the sediment distribution should be coarser after a debris cone. However, our case shows that the grains are rather finer after a debris cone but it is also not clear how the grains on the cones themselves are distributed. They might consist of much more fine grain material than coarse material which would lead to a finer grain size distribution after the cone.

The uncertainties related to the grains in a river bed should not be neglected in the evaluation. First, it has to be defined, whether the line-by-number analysis is carried out on a gravel bar, on a side-arm of the river with a roof-tile like alignment of the grains or on a moving bedload bar. The grain size distributions of those three layer types vary quite a lot (Figure 26) and they match the usual observed variation as shown in Figure 9.

It is furthermore difficult to give a final statement whether the debris cones have an effect on the grain size distribution of the river. Simply taking grain samples before and after the cones does not give enough information. The grains before and after debris cones might be influenced by other factors such as local flow conditions (return current, hydraulic jumps, sub-

or supercritical flow) and the topography (widening or narrowing of the channel, slope before and after the cone, diffuse lateral sediment inputs which are smaller than debris cones). Those issues were not assessed in the field and the available DEM is not precise enough to extract such aspects.

The grain size distribution of the cones themselves should be assessed and their temporal evolution should be measured with tools (for example measuring the elevation changes of fix-points on each cone or tagging certain grains to see how much they move in a certain time period). The analysis should not only be on the debris cones themselves but also on the surrounding conditions in the river reach with precise leveling of the slope before and after each cone and quantifying the change of the stream width. These results might give a clearer evidence to the relation between the slope and the mean diameter than shown in Figure 26.

4.2 DEM Comparison

4.2.1 DEM Properties

The hydrographs of the flight periods clearly showed that the flow during the surveys for the two elevation models differed significantly. Whereas the DTM-AV was taken during continuously low-flow periods, the LiDAR 2009 survey was taken during much higher discharges (20 m³/s vs. 1.5 - 2 m³/s), resulting in a roughly 0.4 m higher water surface elevation (Chapter 3.2.1).

Furthermore, the drop of the DTM-AV (Figure 30) and the early flight in spring 2003 indicates that during the survey of the DTM-AV there might have been snow cover in the area which would also show an increase in elevation for all points. One should figure out whether the Orthophoto from 2003 (Federal Office of Topography swisstopo, 2008) was taken during the flights or whether it was recorded separately. This Orthophoto could verify the assumption of snow-cover in the area.

Those two factors (different flow rate, different survey season) are a major source of uncertainty which can be eliminated easily. For a next LiDAR flight, the office in charge should make sure that the surveys are carried out during a low-flow periods in late summer with no snow cover. This would ensure that the elevations of the river bed and its surroundings are correctly measured. Nowadays there are new laser technologies available which allow to measure the depth below the water surface. Otherwise, the application of echo sounding or an acoustic Doppler profiler are possibilities.

At least it can be said that the manually created "River Polygon" matches a bankful discharge, which is a more common way to define the river banks (see Chapter 2.5.4).

4.2.2 Thalweg comparison and DEM differencing

In only six years' time, the DEM differencing resulted in a mean elevation change of -1.78 m which corresponds to some 30 cm/a up to the "Drop point". The literature shows values for larger rivers (Donau, Orth and others) of 2 - 3.5 cm/a (Nachtnebel, 2010) which is one order of magnitude smaller. Another study showed a degradation of the river bed downstream of dams ranging from 1 to 7 meters over time spans ranging from 3 to 30 years (Galay, 1983). The length of degradation ranges from 2.8 to 300 km downstream of the dam, depending on the observed river. Those values lie in the range of the hereby observed degradation over the length of the

reach up to the „Droppoint“, however, the examples by Galay (1983) are much larger than the Spöl (Colorado river (Hoover Dam, Davis Dam and more), Yellow river (Sanmexia Dam) and many others) and their river bed mostly consists of sand and finer gravel. The results by Galay (1983) therefore have to be put into perspective with the hereby observed river Spöl.

Constructing a high dam traps all the bed material coming from upstream. The released water to the downstream river system is sediment free and tends to pick up grains from the river bed. The rate of erosion depends on factors like the available flow, the grain size distribution and the extent of the sub-surface layer. Up to a certain distance the river is capable to carry the grains as moving bedload or suspended load but as soon as the slope gets smaller or the channel widens and therefore decreases the flow velocity and the shear stress, the sediments will be deposited. This pattern is clearly observable in the DEM differences.

To discuss the origin of the high erosion rate of - 1.78 m, one has to look in the history of the sediment transport in the study area. During the period from 1974 to 1999, there were only a few cases where the flow in the river could mobilize the sediments ($Q > 5 \text{ m}^3/\text{s}$). The numerous debris cones brought a lot of sediment into the river bed, mostly due to precipitation. Snow, ice and wind led to physical weathering and therefore broke up the grains into smaller diameters. As soon as the regular flooding program started in the year 2000, the aggraded grains over the whole reach were now mobilized in each flood event. The first DEM, the DTM-AV was recorded in an early stage of the flooding program leading to the assumption that many of the aggraded sediments from the low-flow period (1974 – 1999) were still present in the system and have not been flushed out of the observed reach. This could explain the high erosion rates up to 2009. When such an analysis would be repeated for the next period of six years (2009 – 2015), the erosion rate would most probably be smaller.

4.2.3 Mass balance comparison

The sediment mass balance Equation 28 showed a large deficit in sediment up to the „Droppoint“, where the DEM Differencing showed a net sediment loss of $-108'554 \text{ m}^3$ which is a high value for such a narrow river and a distance of 4900 m. For the full extent, which is close to 6 km long, a sediment loss of $-26'847 \text{ m}^3$ was determined. Those values can be compared to the study by Lane et al (2003) where a different type of river was analyzed (large, braided river, 1 km wide and 3.3 km long). Lane used the same technique to determine volume changes and the observed volume change in this reach was 170330 m^3 in a period of one month only. This comparison indicates that the gathered values, which stand for the volume change over six years, are in a reasonable range.

4.2.4 Methodical constraints and uncertainties

a) Thalweg comparison

The methods to compare the two Thalwegs was from a topographical point of view not fully accurate. Both extracted river polylines were compared on their relative distance from top to bottom of the reach (0 – 100%). This relative distance was then again projected to the Centerline which was used for the 1D model. This resulted in errors as shown in Figure 41.

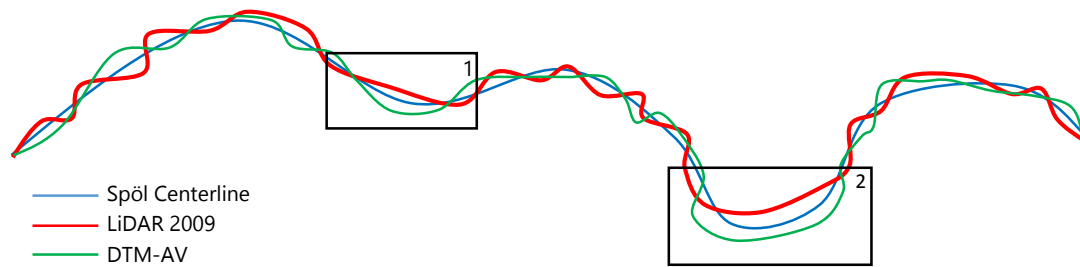


Figure 41: Errors of Thalweg comparison

As the black rectangles 1 and 2 show, each extracted river polyline can have large local discrepancies to the centerline which results in large local deviations in x-direction from the actual point. The Thalweg only represents a small part of a river, namely its steepest point. The DEMs which were used for the comparison had to be filled to do the extraction and therefore the potential sinks which could not be shown with this method.

b) DEM Differencing

The error propagation calculation that has been done for the 2D DEM differencing did only show the measurement errors of the elevation models but not the other effects which increase the uncertainty like different water surface elevations or snow-cover which are described in Chapter 4.2.1. Furthermore the "River Polygon" which was used as a boundary for the DEM Differencing was manually created and the definition of this Polygon could include some cells where there already is a hillslope and no channel and it can also ignore cells which actually are a channel but which were assumed to be a hillslope.

4.3 Basement 1D Model

4.3.1 Simulations

The steady state runs showed that the river bed stays more or less stable up to a discharge of around $5 \text{ m}^3/\text{s}$. This is a lower value than predicted by former expertise ($15 \text{ m}^3/\text{s}$, (Mürle, et al., 2005)). It was also observed in the field that the stones of the armoring layer in the river bed were fully overgrown by algae, which means that the stones in the river bed are not moved and stay on the place during low-flow periods.

The large dimension of algae growth observed in the field might partly be due to the accident that happened in spring 2013 (NZZ, 2013) where a large amount of fine sediment was clogging the whole river bed, offering a lot of nutrients for algal growth. Even after a large flush at the Spöl in Summer 2013 with a peak flow rate of over $75 \text{ m}^3/\text{s}$, there are still many places in the river where the fine sediment can be found, especially in return-flow regions.

Furthermore it shows that it was reasonable to cut all the values below $1.5 \text{ m}^3/\text{s}$ in the hydrograph for the simulations because there is no large scale movement apparent.

The transient runs showed that the limits of the new environmental flow regulation of $10 - 30 \text{ m}^3/\text{s}$ (see Table 2) are chosen reasonably. It correlates with the range where Figure 39 shows the most variations in the maximum and minimum elevation change. However in the last years the floods very often showed a peak which was above $30 \text{ m}^3/\text{s}$. Such high floods do not really have beneficial effects to sediment dynamics (creation of alternating banks, creating pools and riffles, etc.); they only wash out more material.

The total bed load transport showed a gradual increase with higher discharges for the extent of the “Droppoint” whereas on the full extent, the values stayed more or less constant up to a peak flood of $60 \text{ m}^3/\text{s}$ where it seemed that a certain threshold was reached in the last part of the river and the additional sediment coming from upstream was also washed out of the system and not deposited on the last kilometer.

Due to the flood wave propagation along the river reach, the wave looks different on the lower part of the reach than right after its release at the dam Punt dal Gall. The wave is spreading over a longer time span and has a lower peak. With this in mind it is possible to explain the threshold in the last part of the reach. In this case, the sediment transport related Shields parameter θ_{cr} can only be exceeded when a very high peak flood is released from the dam.

The values for the sediment which is flushed out of the system might be used for quantifying the amount of aggradation that is present in the reservoir Ova Spin. However, the downstream boundary conditions which influence the water level downstream of the observed reach should also be included in this analysis as they have a large influence to the flow dynamics. Furthermore, there might also be sediment which gets flushed out from the tributary Ova il Fuorn.

4.3.2 Methodical constraints

The calibration with the DEM differences showed the limitations of this method. It was not clear whether the trends (erosion and deposition) should be better reproduced or if it should be tried to get the same volumes. The time period for the calibration was very long (6 years) and for such a long time series, the cutting of the hydrograph might lead to unreasonable flow conditions where one flood chases the other. In between the floods, there was no period which could be used to build up a new armoring layer in the river.

On the other hand it was not possible to run the whole hydrograph without cutting it because firstly, Basement wouldn't have taken the input file and secondly, the simulation time would have been too long.

The calibration of the model was only partly satisfying because the three goodness-of-fit criteria did not end up in a range where one would expect them to be. At least, the visual judgment showed some correlation between the DEM differences and the model results.

5 Conclusion and Outlook

5.1 Line-by-number analysis

The case study showed that it is possible to show the spatial changes of the grain size distribution in the river Spöl. The line-by-number analysis was for this case a very useful tool. However, the influence of the debris cones to the river could not fully be answered because the behavior of the debris cones themselves in time and space were unknown.

For a more extensive research, there should be multiple grain size samples taken at each location to improve the accuracy. To better understand the behavior of the debris cones, the local movements of the cones should be measured over a longer time and especially before, during and after a flood event. After a flood event, one could measure the grain size distribution on a location that was covered with water and on a location above this point and

determine the difference. Also, other parameters like the slope, the topography (widening or narrowing of the channel) and the flow conditions (backwater flow, hydraulic jumps etc.) should be assessed more detailed.

5.2 Digital elevation models

Concerning the erosion or deposition that occur in the system, two different ways of quantifying the changes were used. The 2D DEM Differencing showed that most of the river was in an erosional state with only a few zones which were uncertain or showed an aggradation. The error propagation calculation showed a relatively small measurement error of less than one meter between the two elevation models. However, many other uncertainties which are present in the system were not included in this error propagation because they could not be quantified.

The Thalweg extraction showed its limitations in the way that the extracted Polylines each followed a different path, which made a proper comparison of two Thalwegs difficult. However, the results showed similarities to the more advanced comparison.

This case study relied heavily on the accuracy of the available Digital Elevation Models. During the study it became clear that both elevation models have their downsides with one being surveyed at various times (DTM-AV) and either with an error or with snow cover causing deviations. The other DEM (LiDAR 2009) was surveyed during a flood which shows significant water heads and therefore influenced the results. For further DEM surveys it should be ensured that there are low-flow conditions and no snow cover. The surveys should be accompanied by an Orthophoto to see the actual surface condition. If this is not possible, other measurement techniques (echo sounding, acoustic Doppler profiler) might be an option. The Swiss Federal Office of Topography will carry out a flight survey in the year 2015 in the framework of a regular swissAlti3D update. As soon as this, renewed, swissALTI3D Elevation Model will be available, similar DEM comparisons should be carried out. They could show whether the hereby observed erosion trends are continued.

5.3 Basement

The 1D model created in Basement could use the previously determined mean roughness coefficient which was determined in the line-by-number analysis. The 1D model showed reasonable results even though oscillations were still present at some local points. For further model generations in this catchment, one should apply a 2D model so that the definitions of the bottom range could be omitted and the grid could easily be coarsened or refined. One could also think about a coupled 1D/2D model because in some points the river does not have enough space for any lateral movements and the computational effort would be reduced.

The extraction of the geometry from the Digital Elevation Model was however difficult because it had to be converted from one software tool to the other. This was coupled with a loss of information. More comments on the modeling software Basement are written in Appendix Chapter 6.2.

For a further analysis, the model should be extended until it reaches the level of the reservoir Ova Spin which means that the downstream boundary condition could be applied. This would also improve the numerical stability. The lateral inflows (at least the flow at Val d'Acqua and

when extending the model, the flow of the river Ova il Fuorn) should be added to the model. There should be discharge measurements carried out in regular intervals in those tributaries to see whether the inflows have an effect or if they can be neglected.

If time allows it, a sensitivity analysis should be carried out in order to see which parameter has the largest influence to the processes and therefore has to be chosen carefully.

One important issue is that there should be easy repeatable measurements available which would allow for a better calibration of the model. The timespan of the calibration should not be six years but rather one flood event or one long period of low flow. Furthermore one should be able to quantify the amount of sediment that is flushed out from the dam Punt dal Gall in an artificial flooding.

6 Appendix

ETH Zürich
Professur für Wasserbau

Flussbau
Dr. G.R. Bezzola

Formular zur Durchführung von Linienproben

Geschiebeanalyse: _____ Datum: _____

Linienprobe Nr.: _____ Beobachter: _____

Standort: _____

Klassengrenzen d_i [cm]	Anzahl Körner								n_i	$\Delta q_i =$ $n_i / \Sigma n_i$	$q_i =$ $\Sigma \Delta q_i$
	5	10	15	20	25	30	35	40			
1 – 2											
2 – 3											
3 – 4											
4 – 6											
6 – 8											
8 – 10											
10 – 12											
12 – 15											
15 – 20											
20 – 25											
25 – 30											
30 – 35											
35 – 40											
40 – 50											
50 – 60											
60 – 80											
80 – 100											
100 – 120											
120 – 150											
150 – 200											
> 200											
									$\Sigma n_i =$		

$d_{max} =$ _____ [cm]

Figure 42: Blank form for the field survey of the line-by-number-analysis

Sediment dynamics modelling in the river Spöl in the Swiss National Park

Table 12: Example of a transformation and evaluation of a line-by-number sample (9B)

LBNA	9B	Date	17.10.2013 GPS 82
Description GB in the middle of the stream, ahead of AF9			

GB	Gravel Bank	u
AF	Alluvial Fan	u+1
r	right	
l	left	

Class threshold		No. Of Grains						Vol. portion	Corr. Cum. Freq								Grain size distribution
d _i [cm]	d _i [cm]	d [cm]	n _i [-]	Δq _i [-]	q _i	Δq _i * d _m ^{0.8}	Δp _i [-]	p _i [-]	p _{ic} [-]	P _{FU(i+1)} [-]	P _{FU(i)} [-]	D _{i, final} [-]	ΔD _{i, final} [-]	d _m *ΔD _{i, final}			
	0		0.05									0.00	0.00	0.00		d10	0.17
	0.1		0.175									0.10	0.10	0.10	0.01	d30	1.30
	0.25		0.375									0.16	0.16	0.06	0.01	d50	3.90
	0.5		0.75									0.23	0.23	0.07	0.03	d70	5.75
1-2	1		1.5	38	0.26	0.26	0.36	0.13	0.13			0.33	0.33	0.10	0.07	d90	11.10
2-3	2		2.5	43	0.29	0.55	0.60	0.22	0.35	0.35		0.46	0.46	0.14	0.20		
3-4	3		3.5	28	0.19	0.74	0.52	0.19	0.54	0.51	0.42	0.56	0.56	0.10	0.26		
4-6	4		5	19	0.13	0.86	0.47	0.17	0.71	0.65	0.59	0.65	0.65	0.09	0.31		
6-8	6		7	8	0.05	0.92	0.26	0.09	0.80	0.78	0.80	0.80	0.78	0.13	0.63		
8-10	8		9	7	0.05	0.97	0.27	0.10	0.90	0.85	0.90	0.92	0.85	0.07	0.49		
10-12	10		11	2	0.01	0.98	0.09	0.03	0.93	0.92	0.95	1.03	0.92	0.07	0.67		
12-15	12		13.5	1	0.01	0.99	0.05	0.02	0.95	0.95	1.01	1.13	0.95	0.03	0.28		
15-20	15		17.5	2	0.01	1.00	0.13	0.05	1.00	0.96	1.06	1.26	0.96	0.01	0.20		
20-25	20		22.5		0.00	1.00	0.00	0.00	1.00	1.00	1.11	1.46	1.00	0.04	0.64		
25-30	25		27.5		0.00	1.00	0.00	0.00	1.00	1.00	1.12	1.63	1.00	0.00	0.00		
30-35	30		32.5		0.00	1.00	0.00	0.00	1.00	1.00	1.10	1.79	1.00	0.00	0.00		
35-40	35		37.5		0.00	1.00	0.00	0.00	1.00	1.00	1.08	1.93	1.00	0.00	0.00		
40-50	40		45		0.00	1.00	0.00	0.00	1.00	1.00	1.07	2.06	1.00	0.00	0.00		
50-60	50		55		0.00	1.00	0.00	0.00	1.00	1.00	1.12	2.31	1.00	0.00	0.00		
		TOTAL			148		2.75										

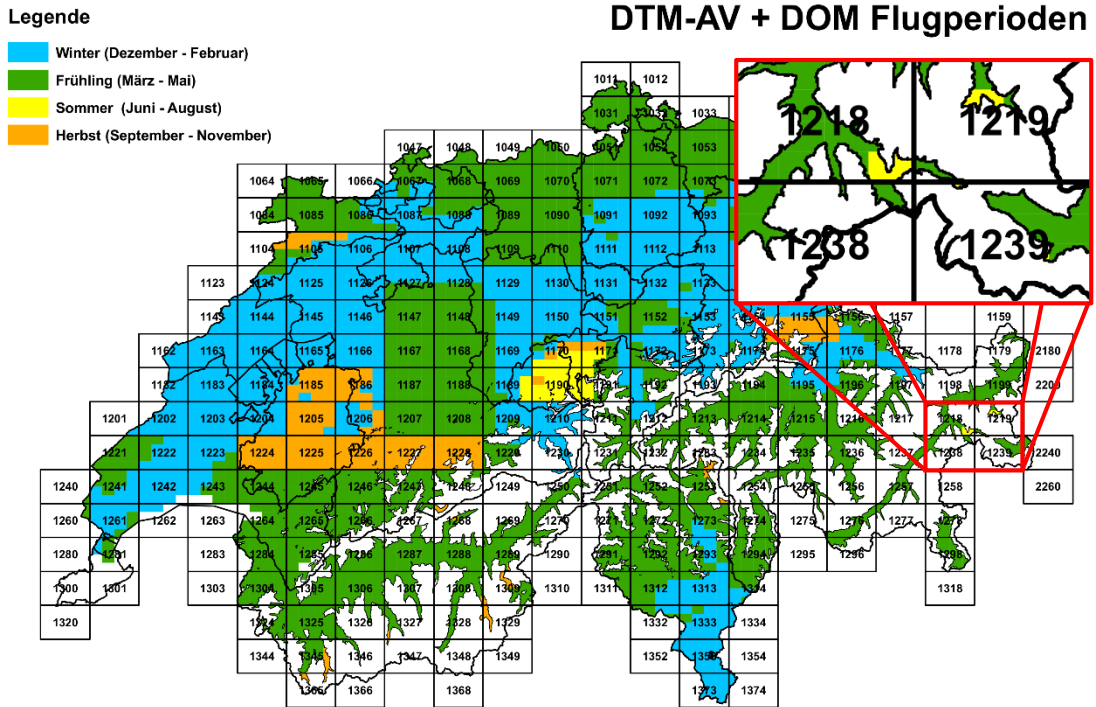


Figure 43: Flight periods of the DTM-AV with a cutout of the study area

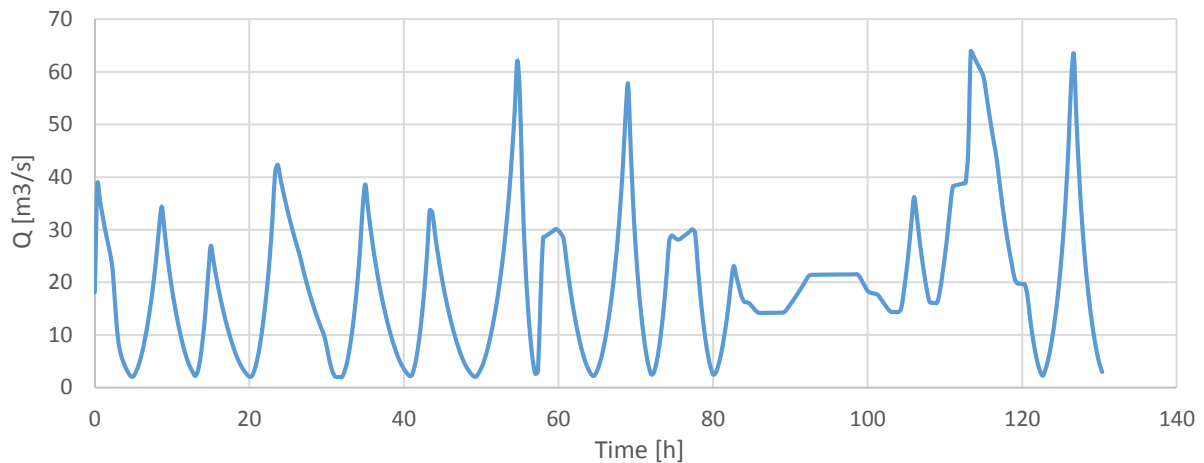


Figure 44: Hydrograph of the floods between 2003 and 2009, cut with all the discharges below 2 m³/s

6.1 Basement Calibration Code

Following the code that was used for the various steady-state and transient case runs:

```

title = Sim127
author = mpfaeffl
date = 11.12.2013
}
DOMAIN {
  multiregion = Sim127
  PARALLEL {
    number_threads = 4
  }
  PHYSICAL_PROPERTIES {
    gravity = 9.81
    viscosity = 1.004e-06
    rho_fluid = 1000
  }
  BASECHAIN_1D {
    region_name = SpoelReach
    GEOMETRY {
      type = basement
      file = Spoel_Geometry_LessNodes_adjusted.bmg
      cross_section_order = (CS1 CS2 CS3 CS4 CS5 CS6 CS7 CS8 CS9 CS10 CS11 CS12 CS13
CS14 CS15 CS16 CS17 CS18 CS19 CS20 CS21 CS22 CS23 CS24 CS25 CS26 CS27 CS28 CS29 CS30 CS31 CS32 CS33
CS34 CS35 CS36 CS37 CS38 CS39 CS40 CS41 CS42 CS43 CS44 CS45 CS46 CS47 CS48 CS49 CS50 CS51 CS52 CS53
CS54 CS55 CS56 CS57 CS58 CS59 CS60 CS61 CS62 CS63 CS64 CS65 CS66 CS67 CS68 CS69 CS70 CS71 CS72 CS73
CS74 CS75 CS76 CS77 CS78 CS79 CS80 CS81 CS82 CS83 CS84 CS85 CS86 CS87 CS88 CS89 CS90 CS91 CS92 CS93
CS94 CS95 CS96 CS97 CS98 CS99 CS100 CS101 CS102 CS103 CS104 CS105 CS106 CS107 CS108 CS109 CS110 CS111
CS112 CS113)
    }
  }
  TIMESTEP {
    CFL = 0.95
    total_run_time = 469200
    initial_time_step = 3
    maximum_time_step = 250
  }
  HYDRAULICS {
    BOUNDARY {
      type = hydrograph
      string = upstream
      file = Above2_20min_Total.txt
      precision = 0.001
      number_of_iterations = 250
      slope = 15
    }
    BOUNDARY {
      type = hqrelation
      string = downstream
      slope = 13
    }
    INITIAL {
      type = fileinput
      file = SpoelInitial.dat
    }
    FRICTION {
      type = strickler
      default_friction = 34.2
    }
    PARAMETER {
      minimum_water_depth = 0.06
      SECTION_COMPUTATION {
        type = table
        min_interval = 0.0025
        max_interval = 0.2025
      }
    }
  }
  MORPHOLOGY {
    PARAMETER {
      density = 2650
      control_volume_type = constant
      porosity = 0.35
      max_dz_table = 0.1
    }
  }
}

```

```

        control_volume_thickness = 1.15
    }
    BEDMATERIAL {
        GRAIN_CLASS {
            diameters = (2 13 39 58 111)
        }
        MIXTURE {
            name = unique
            volume_fraction = (20 20 20 20 20)
        }
        SOIL_DEF {
            name = fixed
        }
        SOIL_DEF {
            name = mobile
            LAYER {
                bottom_elevation = -5
                mixture = unique
            }
        }
        SOIL_ASSIGNMENT {
            type = index_table
            index = (1 2)
            soil = (fixed mobile)
        }
    }
    BEDLOAD {
        PARAMETER {
            bedload_transport = wu
            upwind = 0.5
            theta_critic = 0.045
            bedload_factor = 1.8
            hiding_exponent = -0.6
            local_slope = on
        }
        BOUNDARY {
            type = IODown
            string = downstream
        }
        BOUNDARY {
            type = sediment_discharge
            string = upstream
            file = Upstream_Sediment_Input.txt
            mixture = unique
        }
    }
}
OUTPUT {
    output_time_step = 20000
    SPECIAL_OUTPUT {
        type = tecplot_all
        output_time_step = 469200
    }
    SPECIAL_OUTPUT {
        type = delta_v_sed
        output_time_step = 469200
    }
    SPECIAL_OUTPUT {
        type = monitor
        Qb = (sum)
        cross_sections = (CS81 CS113)
        output_time_step = 469200
    }
}
}
}

```

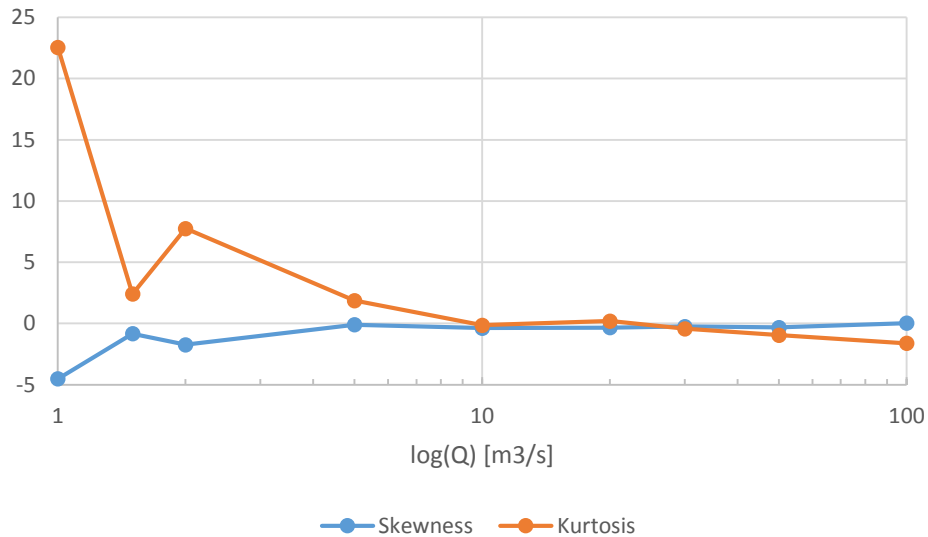


Figure 45: Skewness and Kurtosis for steady-state runs with different discharges

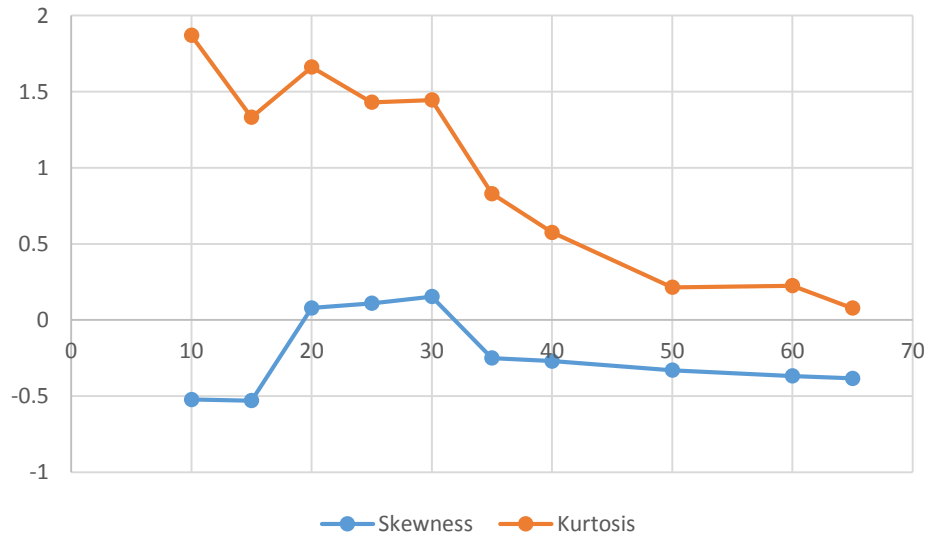


Figure 46: Skewness and Kurtosis for the transient case flood runs with different peak discharges

6.2 Comments to the Software

Some general comments about the modeling software Basement with the 1D module BASEchain are outlined here. The 1D simulation in Basement needs a specific geometry file which is not in a common format that can be generated or read by the most used geographical software. If cross-sections have to be derived from a Digital Elevation Model, one is limited to the use of HEC-GeoRAS and HEC-RAS which is itself also a 1D model for sediment transport. Once the geometry file is in Basement, most modifications have to be adapted manually in the code. Basement lacks a wide range of tools in the geometry editor which would save a lot of time. Some ideas for further development are:

- The HECRAS2Basement python script should be able to take multiple roughness values for the left and the right overbank.
- A tool to add the soil definition to every cross-section and assign them values, like set value to 2 for cross-sections 2 – 112. The extent of the soil definition might be estimated

due to a hillslope change where it automatically detects the last point of the river bed next to the left and right bank and therefore makes the manual step of defining this for each cross section redundant.

- A tool that adds the parameter "bottom range" to each cross-section. The extent can be chosen to be taken from other parameters such as the soil definition.
- One the interpolation fix points are estimated by a tool, they give error messages when deleting nodes manually in a cross-section even after the fix points have been removed. They have to be added (then an empty bracket appear in the code) and deleted again in order for not having an error message in the geometry.
- The calculations which are defined in Figure 21 should be altered in a way that the fix point nodes with which the sediment dynamics are calculated can be altered according to the flow in the bed. An amendment in BASEchain to solve this problem is already planned and will most probably be released in February 2014.
- It should be possible to have shape files as an output file which can directly be imported to ArcGIS or any other Geographical Information System.
- Basement should handle flow hydrographs with more rows. It crashed with a text-file that contained 821 rows but worked for one with 420 rows.
- Last but not least it should be assured that the program works on all current machines, including Windows 8.1.

7 List of Figures

Figure 1: Hydrograph before and after dam construction and with improved environmental flow regulations (Noack, 2012).....	5
Figure 2: Overview of the study site including the hydropower infrastructure (Mürle, 2000)	7
Figure 3: Various debris cones (upper left: DC8, upper right: DC5, lower: DC3)	8
Figure 4: Riffle-pool-sequence in the upper part of the reach	9
Figure 5: Channel widening with gravel bar.....	9
Figure 6: Algae growth in a return flow area	10
Figure 7: Canyon like section near the End of the reach	10
Figure 8: Armoring layer and sub-surface layer of a gravel-carrying river bed. (Patt, et al., 2011)	11
Figure 9: Grain size distribution of different river bed layers	12
Figure 10: Balance of forces for a single particle (Janssen, 2010)	14
Figure 11: Shields diagram (vit13).....	14
Figure 12: Definition of exposure height of bed material (Wu, et al., 2010).....	15
Figure 13: Overview of the river reach with the acquired grain size samples and the observed debris cones (Map: Orthophoto Ova Spin, © bsf swissphoto.....	20
Figure 14: Hydrograph of Station "Punt dal Gall" from May - September 2003.....	22
Figure 15: Hydrograph of Station "Punt dal Gall" from June 19 -20, 2009	22
Figure 16: Flow Direction calculation steps (ESRI).....	23
Figure 17: Extract of the river Spöl, showing fluctuating Thalwegs and the defined Stream Centerline (Map: LiDAR Ova Spin © bsf swissphoto).....	24
Figure 18: Custom model for DEM comparison in ArcGIS.....	25
Figure 19: Cross sections extracted with HEC-GeoRAS.....	29
Figure 20: Effect of bed load on cross-section geometry (Laboratory of Hydraulics, Hydrology and Glaciology, 2013)	30
Figure 21: Deposition a) and erosion b) due to bedload with cross section points on embankments. (Laboratory of Hydraulics, Hydrology and Glaciology, 2013).....	31
Figure 22: Raw (left) and modified (right) geometry of cross-section 13 (Basement)	31
Figure 23: Steady-state run with 15 m ³ /s, single grain size, 2.3 days.....	34
Figure 24: Synthetic floods with different peaks for a duration of 30000 s (8.3 hours) and low flow of 70000 s (19.4 hours)	36
Figure 25: Overview of the line-by-number analysis samples across the river reach. The points describe the sample values obtained and the lines describe the mean value from the first sample after a debris cone up to the next cone. The cones are indicated as a gradient line...37	37
Figure 26: Grain size distribution variations depending on layer type, shown as a weight fraction q_i [-]. The layers described are taken from specific sample distributions observed in the field.	38
Figure 27: Relationship between mean grain diameter d_m and slope J	39
Figure 28: Histogram of k_{st} values for the reach in the Spöl.....	39
Figure 29: Kriging interpolation of river reach. (Maps: LiDAR 2009 © bfs swissphoto, DTM-AV © swisstopo)	40

Figure 30: Different Thalwegs extracted from the DEMs DTM-AV (2003) and LiDAR (2009). The "Droppoint" shows a point where the DTM-AV drops around 10 m and stays constant from this point on.....	41
Figure 31: Negative, neutral and positive elevation changes for the river reach Spöl (Maps: LiDAR 2009 © bfs swissphoto, DTM-AV © Swisstopo).....	42
Figure 32: Upper part of the reach with deposition (positive, marked green) in the middle of the channel (Maps: LiDAR 2009 © bfs swissphoto, DTM-AV © Swisstopo).....	42
Figure 33: Middle part of the reach with largely erosion (negative, marked red) and some uncertain (neutral, marked yellow) zones at the banks (Maps: LiDAR 2009 © bfs swissphoto, DTM-AV © Swisstopo)	42
Figure 34: Lowermost part of the reach with mostly deposition (positive, marked green) and some uncertain zones (neutral, marked yellow) at the banks (Maps: LiDAR 2009 © bfs swissphoto, DTM-AV © Swisstopo).....	43
Figure 35: Histogram of the differences between LiDAR 2009 and DTM-AV up to the Droppoint (blue bars) and additional orange bars when looking at the full extent.....	43
Figure 36: Mean elevation change for the full extent with min. and max. for each reach in the river Spöl.....	44
Figure 37: Final calibration run with all floods between 2003 and 2009 compared to the DEM-Differences for the full extent.	46
Figure 38: Mean elevation change per day and basic statistics over the whole reach for steady-state flow for the full extent.	47
Figure 39: Mean elevation changes for each flood and basic statistics.....	47
Figure 40: Total bed load transport (Q_b) for various flood events once to the "Droppoint" and once for the full extent.	48
Figure 41: Errors of Thalweg comparison.....	52
Figure 42: Blank form for the field survey of the line-by-number-analysis.....	56
Figure 43: Flight periods of the DTM-AV with a cutout of the study area	58
Figure 44: Hydrograph of the floods between 2003 and 2009, cut with all the discharges below 2 m ³ /s.....	58
Figure 45: Skewness and Kurtosis for steady-state runs with different discharges.....	61
Figure 46: Skewness and Kurtosis for the transient case flood runs with different peak discharges.....	61

8 List of Tables

Table 1: Environmental flow releases in the river Spöl since 1970	4
Table 2: Recommendation for modified environmental flow release	5
Table 3: Overview of the flights for the DTM-AV DEM	17
Table 4: Overview and properties of the available DEMs in the project area.....	17
Table 5: Assigned roughness to habitat classes (PSW, D.R. Knauf)	29
Table 6: Range of goodness for the Nash-Sutcliffe criterion.....	33
Table 7: Relative change of the grain size diameter at each debris cone.....	37
Table 8: Basic statistics of the line-by-number analysis with the mean grain diameter d_m and the characteristic diameter d_{90} for the sub-surface layer.....	38
Table 9: Basic statistics of the differences between LiDAR 2009 and the DTM-AV up to the "Droppoint" and for the full extent.....	44

Table 10: Covered Area (how many cells are defined as uncertain, negative or positive) and sum of volume in m ³ for each class calculated for the full extent and up to the "Droppoint"	45
Table 11: Goodness of fit criteria and volume change for the calibration of the 1D model up to the "Droppoint" and for the full extent.....	46
Table 12: Example of a transformation and evaluation of a line-by-number sample (9B).....	57

9 Literature

Bezzola Gian Reto Flussbau, Vorlesungsmanuskript [Book]. - Zürich : Versuchsanstalt für Wasserbau, ETH Zürich, 2013. - Vol. FS 2013.

Dusza Przemyslaw Mosaikierung eines neuen digitalen Geländemodells [Report]. - Zerneux : Schweizerischer Nationalpark, 2010.

EAWAG Wasser und Energie - Faktenblatt. - Dübendorf : [s.n.], September 2011.

ESRI ArcGIS Webhelp [Online]. - November 2013, 2013. - http://webhelp.esri.com/arcgisdesktop/9.3/published_images/SAC_Hydro_Flow_direction.gif.

Federal Office of Topography swisstopo Alte SWISSIMAGE Farborthophotos, Übersichten der verfügbaren Bilder (pro Jahr) [Online]. - March 10, 2008. - December 06, 2013. - <http://www.swisstopo.admin.ch/internet/swisstopo/de/home/products/images/ortho/swissimage.parsysrelated1.76752.downloadList.82455.DownloadFile.tmp/swissimage9805.pdf>.

Fehr René Einfache Bestimmung der Korngrößenverteilung von Geschiebematerial mit Hilfe der Linienzahlanalyse [Journal] // Schweizer Ingenieur und Architekt, Abwassertechnik / Wasserbau. - Zürich : [s.n.], 1987. - 38/87. - pp. 1104 - 1109.

Galay V.J. Causes of River Bed Degradation [Article] // Water Resources Research. - North Vancouver : Northwest Hydraulic Consultants, October 1983. - 19. - No 5. - pp. 1057-1090.

Janssen Stephan R. A part of Transport: Testing sediment transport models under partial transport conditions [Report] / Water Engineering and Management. - Enschede : University of Twente, 2010.

Laboratory of Hydraulics, Hydrology and Glaciology System Manuals of BASEMENT [Book]. - Zurich : ETH Zurich, 2013. - 2.3 : Vol. Version 2.3.

Lane Stuart N, Westaway Richard M. and Hicks D. Murray Estimation of erosion and deposition volumes in a large, gravel-bed, braided river using synoptic remote sensing [Article] // Earth Surface Processes and Landforms 28 / ed. InterScience Wiley. - 2003. - pp. 249-271.

Molnar Peter Fluvial System Lecture Notes. - [s.l.] : ETH Zurich, 2012.

Mürle Uta Morphologie und Habitatstruktur in der Ausleitungsstrecke einer alpinen Stauhaltung (Spöl, Schweizerischer Nationalpark, Engadin) [Report]. - Öschelbronn : Institut für Geographie und Geoökologie Universität Karlsruhe TH, 2000.

Mürle Uta, Ortlepp Johannes and Molinari Peter Die Dynamisierung des Restwassers im Spöl - eine Win-Win-Lösung für Natur und Kraftwerksbetreiber [Journal]. - Baden : Wasser Energie Luft, 2005. - 1/2-2005.

Nachtnebel H.P. Gutachten zur UVE Flussbauliches Gesamtprojekt östlich von Wien [Report]. - Wien : N.Ö. Umweltschutz, 2010.

Noack Markus Modelling Approach for Interstitial Sediment Dynamics and Reproduction of Gravel-Spawning Fish [Article] // Mitteilungen. - Stuttgart : Institut für Wasser- und Umweltsystemmodellierung der Universität Stuttgart, 2012. - Vol. Heft 214.

NZZ Stausee-Unfall im Nationalpark, Aufbauarbeiten am Spöl beginnen von Neuem [Journal]. - Zürich : Neue Zürcher Zeitung, Markus Hofmann, April 3, 2013.

Patt Heinz and Gonsowski Peter Wasserbau; Grundlagen, Gestaltung von wasserbaulichen Bauwerken und Anlagen, 7. Edition [Book]. - Berlin Heidelberg : Springer-Verlag, 2011.

PSW, D.R. Knauf Programm Service Wasserwirtschaft, Rauheitsklassen für Gewässer [Online]. - November 02, 2013. - <http://www.psw-knauf.de/download/Gewaesser-Rauheiten.pdf>.

Rosgen David L A classification of natural rivers // Wildland Hydrology. - Pagosa Springs : [s.n.], 1994.

Swiss Federal Agency Abkommen zwischen der Schweizerischen Eidgenossenschaft und der Italienischen Republik über die Nutzbarmachung der Wasserkraft des Spöl // SR 0.721.809.454.1. - Bern : [s.n.], May 27, 1957.

Swiss Federal Office of Energy Faktenblatt Restwassersanierung Spöl. - September 2, 2011.

Swiss Federal Office of Energy Schweizerische Gesamtenergiestatistik 2012 [Report]. - Bern : SFOE, 2012.

Swiss National Park Basisprospekt. - Zernez : [s.n.], 2013.

Swiss National Park www.parks.ch [Online]. - 12 08, 2013. - <https://www.parks.ch/snp/maindata/Habitat.htm#fgdcMetadata>.

Taylor John R An introduction to Error Analysis: The study of uncertainties in physical measurements, second edition [Book]. - Sausalito, California : University Science Books, 1997.

vit.bme.hu [Online]. - December 07, 2013. - http://vit.bme.hu/targyak/mundus_3rd/vedett/sediment/shields_diagram.jpg.

Wu Weiming, Wang Sam S.Y. and Jia Yafei Nonuniform sediment transport in alluvial rivers [Article] // Journal of Hydraulic Research. - London : National Center for Computational Hydroscience and Engineering, School of Engineering, University of Mississippi, 2010.

Declaration of Originality

This sheet must be signed and enclosed with every piece of written work submitted at ETH.

I hereby declare that the written work I have submitted entitled

Sediment dynamics modelling in the river Spöl in the Swiss National Park

is original work which I alone have authored and which is written in my own words.*

Author(s)

Last name
Pfäffli

First name
Matthias

Supervising lecturer

Last name
Molnar

First name
Peter

With the signature I declare that I have been informed regarding normal academic citation rules and that I have read and understood the information on 'Citation etiquette' (http://www.ethz.ch/students/exams/plagiarism_s_en.pdf). The citation conventions usual to the discipline in question here have been respected.

The above written work may be tested electronically for plagiarism.

Zurich, 20.12.2013

Place and date

M. Pfäffli

Signature